

Sulfidization in a shallow coastal depositional setting: diagenetic and palaeoclimatic implications

*A.Mazumdar**, *A. Peketi*, *H. Joao*, *P. Dewangan*, *D.V. Borole*, *M. Kocherla*

Geological Oceanography

National Institute of Oceanography

Donapaula, Goa-403004

*for correspondence *maninda@nio.org*

Abstract

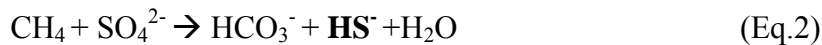
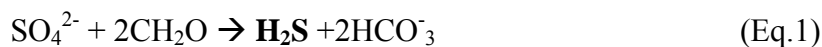
The inner shelf off west coast of India, is covered with late Holocene to recent organic rich, silty-clay dominant sediments. High TOC content and sedimentation rates result in high sulfate reduction rates in this region (Mazumdar et al., 2009). In the present study, we have investigated the nature of pyrite and C-Fe-S geochemistry in a sediment core (covering the last 378 y) at a water depth of 17 m off Goa, west coast, India, to understand the diagenetic and palaeoclimatic/oceanographic processes. The chromium reducible sulfur (CRS) and highly reactive iron (Fe_{HR}) profiles show significant fluctuations and a negative correlation with $\delta^{34}S_{CRS}$, which is attributed to relative availability of highly reactive and less reactive iron bearing minerals close to the sediment water interface. Low $\delta^{34}S_{CRS}$ corresponding to high CRS content characterizes early diagenetic pyritization near the sediment-water interface, whereas high $\delta^{34}S_{CRS}$ and low CRS content indicate late diagenetic pyritization of less reactive iron during burial. High OBS/CRS ratios suggest the important role played by the labile organic compound in binding sulfur in the sediment. Partitioning of stable sulfur isotopes into organic and iron bound phases is apparently linked to Fe_{HR} and labile organic matter availability. We have proposed Fe_{HR} profile and Fe_{HR}/Fe_T ratios as a potential tool to understand runoff /monsoonal fluctuations in a shallow marine depositional setting. To develop this tool into a potential paleoclimatic/ oceanographic proxy and to link it to other proxies within a chronological framework, needs high resolution sampling and age dating.

Keywords: Pyrite Framboid, Reactive iron, Organic bound sulfur, Chromium reducible sulfur, Sulfur isotope.

1. Introduction

Dissimilatory sulfate (SO_4^{2-}) reduction (Harrison and Thode, 1958; Sweeney and Kaplan, 1980; Jørgensen, 1990; Madigan et al., 2000; Canfield, 2001; Goldhaber, 2003; Megonigal et al. 2003; Shen and Buick, 2004; Canfield, 2005 and Canfield et al., 2006; Sim et al., 2011) is a bacterially-mediated metabolic process which results in the breakdown of S-O bond of dissolved sulfate and subsequent production of H_2S gas. During this transition, the valence state of sulfur changes from +6 to -2, i.e., a net transfer of 8 electrons via enzymatic pathways (Madigan et al., 2000). Several short lived sulfur compounds of intermediate valence states viz., sulfite (SO_3^{2-}), tetrathionate ($\text{S}_4\text{O}_6^{2-}$), thiosulfate ($\text{S}_2\text{O}_3^{2-}$) and elemental sulfur (S^0) (Zopfi et al., 2004) are known to exist in the sediment pore waters. Dissimilatory sulfate reduction plays an extremely important role in diagenesis of marine sediments and accounts for half or more of total organic carbon mineralization within sediments (Jørgensen, 1982; Canfield, 1989; Kristensen, 2000). Rate of sulfate reduction in marine sediments depends mainly on the availability of labile organic compounds which serve as substrate for sulfate-reducing bacteria (Madigan et al., 2000), temperature (Westrich and Berner, 1988; Madigan et al., 2000; Canfield et al., 2006), bacterial species (Canfield, 2001; Detmers et al., 2001), sedimentation rate (Goldhaber and Kaplan, 1975; Berner, 1978; Canfield 1989; Claypool, 2004) and sulfate concentrations (Canfield, 2005). Sulfate reducing bacteria (SRB) are strict anaerobes and grow only in complete absence of oxygen. SRBs are most active close to sediment water interface owing to high organic load and sulfate flux (Megonigal et al., 2003; Kasten and Jørgensen, 2000). Preservation of labile organic matter and its availability to the sulfate reducers depends on oxygen penetration depth, which in turn is controlled by sedimentation rate and water column oxygen availability (Hedges and Keil, 1995; Gélinas et al., 2001).

Dissimilatory sulfate reduction can be represented by equations 1 to 3.



Free energy yield (ΔG) during sulfate reduction depends on the electron donors (substrate). Fermentation products like acetate, lactate, formate and H_2 are the common substrates in organic rich sediments. Brüchert (2004) compiled the ΔG values (-45 to $-340 \text{ kJmol}^{-1} \text{ SO}_4^{2-}$) for a wide range of substrates amenable to sulfate reduction. Anaerobic methane oxidation (AMO) also plays a profound

role in sulfate reduction. AMO (Eq.2) is believed to be performed by a consortium of CH₄-oxidizing archaea and sulfate-reducing bacteria (SRB) in marine environments (Hoehler and Alperin, 1996; Boetius et al., 2000; Orphan et al., 2001; Valentine, 2002).

A significant fraction of the H₂S produced during the above reactions diffuses out of the sediments and gets oxidized to sulfate or trapped in the bacterial mats as S⁰ (Hansen et al., 1978; Chanton et al., 1987). A fraction of the H₂S is trapped in the sediment as FeS, FeS₂, S⁰ and OBS (organic bound sulfur), out of which, pyrite and OBS are quantitatively the most significant sink of reduced sulfur in the marine environment (Kump and Garrels, 1986; Werne et al., 2003). Sedimentary sulfidization has been studied in a wide variety of depositional environments (Skyring, 1987; Roychoudhury et al., 2003) across the geological time scale (Strauss, 1997).

Mazumdar et al. (2009) reported pore fluid chemistry of 1.5-2 m long sediment cores collected off the coast of Goa, west coast, India. Cores were collected from water depths 16 to 40 m. Sulfate concentration profiles in this region show linear drop with gradients ranging from 0.042 mM/cm to 0.288 mM/cm and the depth integrated sulfate reduction rates range from 0.0018 mmol/cm²/y to 0.0126 mmol/cm²/y. Whereas, the depths of sulfate-methane interface (SMI) vary from 70 to 225 cmbsf. In the present study we have carried out an investigation of the C-Fe-S geochemistry in a sediment core collected at a water depth of 17 m off Goa to understand the nature of pyritization, sulfurization of organic matter, distribution of reactive iron and to test their implications in palaeoclimatic/oceanographic studies.

2. Sedimentation and Hydrography

The inner continental shelf off west coast of India is marked by even and gently sloping topography with slope changing from 1:700 to 1:3300 (Wagle et al., 1994). The inner shelf is covered with a late Holocene to Recent sediment wedge of silt and clay which pinches out at a water depth of 45-50m. Beyond 50m, the sediment is composed predominantly of calcareous oolitic sand (Nair and Pylee, 1969; Nair et al, 1978). The late Holocene sedimentary wedge can be traced all along the west coast (Siddiquie et al., 1981; Karisiddaiah et al., 1993; Karisiddaiah and Veerayya, 1996) and it ranges in width from 175 km (off Narmada-Tapti) to 25 km off Cochin (Rao and Wagle, 1997). Holocene sea level rise (Hashimi, et al., 1995) resulted in the deposition of this organic rich fine grained sediment wedge (Karisiddaiah et al., 2002 and Mazumdar et al., 2009). The wedge shaped sediment cover (high stand system tract) developed on the maximum flooding surface (MFS) around 7000 years BP (Hashimi et al., 1995;

Mazumdar et al., 2009). The sediment cover has parallel continuous reflectors showing a progradational stacking pattern and downlaps onto the MFS. Numerous paleo fluvial channels exist under the transgressive surface (Karisiddaiah et al., 2002). Presence of acoustic blanking suggests the occurrence of shallow gases (Siddiquie et al., 1981; Karisiddaiah, and Veerayya, 1996; Mazumdar et al., 2009).

^{210}Pb -excess ($^{210}\text{Pb}_{\text{xs}}$) based estimation of sedimentation rates off Goa varies significantly. Kurian et al. (2009) estimated a sedimentation rate of 0.15 cm/y at a water depth of 40 m. Nigam et al. (1995) reported a sedimentation rate of 0.26 cm/y at a water depth of 20 m. Sedimentation rates as high as 0.72 and 0.84 cm/y have also been estimated off Goa over water depths of 18 to 20 m (Borole, 2011 *personal communication*).

The west coast experiences strong upwelling of cold, nutrient rich and oxygen depleted water during southwest monsoon (SWM: June-September). This region also receives high rainfall (~3000 mm) during this period resulting in shallow thermohaline stratification. Respiration of excessive organic matter in the water column results in hypoxia and even in free hydrogen sulfide for a limited period (Naqvi et al., 2006). The seasonally occurring natural hypoxic zone occupies an area of about 2,00,000 km², and is the largest of its kind in the world (Naqvi et al., 2000, 2006).

3. Methodology

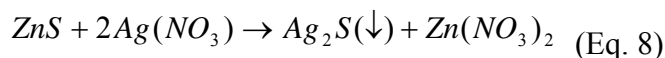
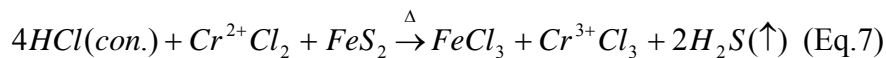
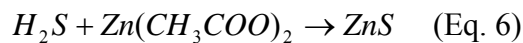
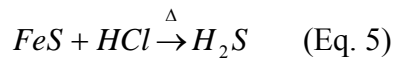
A 1.63 m long gravity core (SASU 97/3: figure-1) was collected at a water depth of 17 m on-board *CRV Sagar Shukti* (SASU-97) in April, 2005 from a location (Lat: 15° 06.93', Long: 73°52.74') off the coast of Goa (Figure-1). Acrylic liner (2m x 5.5 cm) was used for core collection. Measured sediment lengths were extruded from the liner, using a piston, and cut into 5 cm thick slabs within 20-30 minutes of core retrieval. Each slab was immediately transferred into a thick plastic bag, filled with high purity nitrogen and heat sealed to avoid atmospheric oxygen which can oxidize hydrogen sulfide or iron monosulfide. The N₂ filled bags were stored at 2°C prior to pore water extraction. Pore water extraction was carried out using a cryo-centrifuge (Heraeus Biofuge) maintained at 4°C and subsequently filtered through 0.2 micron Whatman syringe filter and stored in crimped vials in a nitrogen atmosphere. Sulfate ion concentrations were measured using a Dionex-600 ion chromatograph (Gieskes et al., 1991). Prior to sample injection, 1 ml of pore water sample was diluted to 50 ml or 100 ml and passed through silver cartridge (Dionex) to remove chloride ion. An IonPac AS9-HC column was used for ion separation and ASRS Ultra-II (2 mm) was used as anion self-regenerating suppressor. Calibration curve was prepared using standard IC sulfate solution from Dionex. BaCl₂ solution was added to the filtered acidified pore

waters to precipitate the dissolved sulfate as BaSO₄. BaSO₄ was recovered by filtration and dried for sulfur isotope ratio measurement.

The measurement of ²¹⁰Pb activity in the core was carried out using the standard procedure (Krishnaswami and Lal, 1978; Sharma et al., 1994; Blaha et al., 2011). An aliquot (2-3 g) of dry sediment was dissolved in a mixture of HF-HClO₄-HNO₃ in the presence of 1 ml ²⁰⁸Po as tracer. A silver planchet was placed in the beaker and plated with dissolved Po isotopes over 3-4 hours. ²¹⁰Pb activity was determined by measuring the alpha activity of ²¹⁰Po using an Ortec-Plus alpha spectrometer (EG & G Ortec). Unsupported ²¹⁰Pb activity (²¹⁰Pb excess) was determined by subtracting the background ²¹⁰Pb activity supported by ²²⁶Ra from the total ²¹⁰Pb activity (Eq. 4). The average sedimentation rate was calculated using the slope of the ²¹⁰Pb_{xs} trend on a semilog plot (Dickin, 1995) and assuming a constant ²¹⁰Pb flux. ²¹⁰Pb has a decay constant of 0.03114 y⁻¹

$$^{210}\text{Pb}_{\text{xs}} = ^{210}\text{Pb}_{\text{total}} - ^{210}\text{Pb}_{\text{supported}} \quad (\text{Eq. 4})$$

Elemental sulfur (S⁰) was removed from an aliquot of homogenized wet sample by shaking it with dichloromethane (Brüchert and Pratt, 1996; Brüchert, 1998) on a vortex shaker for 10 minutes. Dichloromethane extract was separated by centrifugation. Acid volatile sulfide (AVS) and chromium reducible sulfur (CRS~ pyrite) were extracted from the S⁰ free sediment using 6 N HCl and boiling 1 M CrCl₂ (in 6 N HCl) solutions sequentially in an oxygen free reaction vessel with continuous nitrogen flow. H₂S produced by reduction of sulfide was trapped as ZnS in zinc acetate solution (pH>11) and subsequently reprecipitated as Ag₂S by adding AgNO₃ (Canfield et al. 1986). The colloidal suspension of Ag₂S was boiled for ~10 minutes to produce consolidated Ag₂S lumps which are subsequently collected on 0.2 micron nitro cellulose filter paper and washed with distilled water. The Ag₂S lumps were oven dried, weighed and homogenized for isotope ratio measurements. The reactions involved in sulfide extraction are given below.



Organic bound sulfur (OBS) was extracted by combusting the S^0 and sulfide free sediment residue with Eschka's mixture (2:1 mixture by weight of $MgO: Na_2CO_3$) at $850^\circ C$ for an hour (Tuttle et al., 1986). The resulting sulfate was dissolved in hot water and precipitated as $BaSO_4$ by addition of $BaCl_2$. The solution was made acidic to avoid any carbonate precipitation. The suspension containing barium sulfate was boiled for half an hour and then kept at around $90^\circ C$ overnight for coarsening and purification of the $BaSO_4$ crystals (Mazumdar and Strauss, 2006). The $BaSO_4$ precipitate was filtered, dried and weighed for the quantification of OBS.

$\delta^{34}S$, $\delta^{18}O$ of $BaSO_4$ and $\delta^{34}S$ of Ag_2S were measured with a Thermo Delta-V-plus isotope ratio mass spectrometer with continuous flow system and attached with an elemental analyser (Thermo EA1112). $BaSO_4$ and Ag_2S precipitates were mixed with V_2O_5 and combusted at $1150^\circ C$ to produce SO_2 . Whereas oxygen isotope ratio measurement of $BaSO_4$ was carried out following pyrolysis of $BaSO_4$ to CO at $1450^\circ C$ in a glassy carbon reactor of EA1112 elemental analyser. All results are reported in the standard delta notation as permil deviations from the VCDT (Vienna Canyon Diablo Troilite) and VSMOW (Vienna Standard Mean Ocean Water) with reproducibility better than $\pm 0.3\text{‰}$ for S and O isotope ratios. IAEA standards SO-5 ($BaSO_4$: $+0.5\text{‰}$ VCDT, $+12\text{‰}$ VSMOW), SO-6 ($BaSO_4$: -34.1‰ VCDT, -11‰ VSMOW), NBS127 ($BaSO_4$: $+22.3\text{‰}$ VCDT, $+9.3\text{‰}$ VSMOW), S-1 (Ag_2S : -0.3‰ VCDT) and S-2 (Ag_2S : $+22.7\text{‰}$ VCDT) were used for the preparation of calibration curves.

Total carbon (TC) and total nitrogen (TN) contents of sediments were measured by elemental analyzer (Thermo CNS 2500). High purity helium was used as the carrier gas. CO_2 and N_2 were detected by Thermal conductivity detector (TCD). Total inorganic carbon (TIC) was measured by UIC carbon coulometer (CM 5130). Total organic carbon (TOC) was calculated by subtracting TIC from TC. Carbon stable isotope ratio measurement of total organic carbon was carried out using a Thermo-Finnigan Delta-V-Plus continuous flow isotope ratio mass spectrometer attached to an elemental analyzer (Thermo EA1112). The external precision calculated for $\delta^{13}C$ is typically $0.07\text{--}0.09\text{‰}$ (VPDB). Carbon isotope ratios are reported in standard format relative to Vienna Peedee Belemnite (VPDB) standard.

The available reactive iron (ferrihydrite: $FeOOH \cdot 0.4H_2O$ + lepidocrocite: $\gamma\text{-}FeO(OH)$ + goethite $FeO(OH)$ + hematite: Fe_2O_3) in the sediment (Fe_p) was extracted with buffered sodium dithionite solution following Canfield (1989) and Mehra and Jackson (1960). Iron concentrations ($Fe^{3+} + Fe^{2+}$) were measured by ferrozine complexometry following reduction of Fe^{3+} to Fe^{2+} by addition of

hydroxylamine hydrochloride in the leachate. A Chemito spectrophotometer (Spectroscan UV 2700) was used to measure absorbance at 515 nm. The highly reactive iron (Fe_{HR}) is the sum of dithionite bound iron (Fe_D) and pyrite bound iron (Fe_{CRS}). Total iron concentration in freeze dried bulk sediment samples was determined by X-ray Fluorescence (PAN analytical Axios) technique using fused pellets..

Pyrite grains ($\rho \sim 4.8\text{--}5 \text{ g/cm}^3$) were separated from the freeze dried sediment samples by gentle disaggregation using a soft wooden pestle-mortar and subsequently by gravity settling through bromoform ($\rho = 2.78 \text{ g/ml}$). Separated particles were cleaned with 0.1N HCl and repeatedly washed with acetone. Pyrite particles were observed under optical zoom microscope (Leica) and a Jeol scanning electron microscope (SM5800LVJeol).

Gamma density (wet bulk density) of the whole core was measured using a GEOTEK Multisensor Core Logger (MSCL) following standard GEOTEK calibration and measurement protocol (www.geotek.co.uk/ftp/manual.pdf). The porosity (ϕ) can be derived (Eq.9) from the wet bulk density (ρ_{MSCL}) assuming that the sediment is fully saturated with water and the grain ($\rho_s = 2.65 \text{ g/cc}$) and fluid ($\rho_{fl} = 1.03 \text{ g/cc}$) densities are known,

$$\rho_{MSCL} = \phi\rho_{fl} + (1 - \phi)\rho_s \quad (\text{Eq. 9})$$

4. Results

4.1. Age depth model

$^{210}Pb_{xs}$ decline exponentially over a depth of 2.25 to 22.5 cmbsf, yielding an average sedimentation rate of $0.43 \pm 0.0415 \text{ cm/y}$ (Fig.2). The extrapolated age to the depth of 162.5 cm is estimated to be 378 year assuming constant sedimentation rate.

The average porosity of the whole core is $80 \pm 2.38\%$ (supplementary figure 1).

4.2 Pyrite grain morphology

Pyrite grains of different morphological types recovered from the core Sasu-97/3 are presented in figure 3. They include isolated pyrite framboids (Fig. 3A, B, C, D and E), clusters of pyrite framboids (Fig. 3 F) and irregular aggregates (48 to 107 μm) of pyrite crystals (Fig.3 G, J, I, K and L). Framboids range in size from 3.9 to 36 μm and the constituent microcrystals are of 0.4 to 2 μm in diameter. Microcrystals are octahedral and their sizes correlate positively with the framboid diameter (Fig. 4). Pyrite crystals within the large aggregates are cubo-octahedral with highly variable sizes (0.8 to 8.7 μm).

The intra-microcryst space in the framboids show variable amounts of in-filling (Fig. 3B, C, D and E) with later generation pyrite, giving rise to interpenetrating and welded crystals. Calcareous and Opalline tests are often filled with framboids and single pyrite octahedral crystals (Fig.3 C). The filled framboids within the tests show deformation due to growth pressure. A transformation from spherical to polyhedral framboid is also noted in figure-3 D. Titanomagnetite crystal surfaces show dissolution pits (Fig. 3H).

4.3 Sediment Chemistry

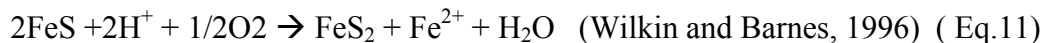
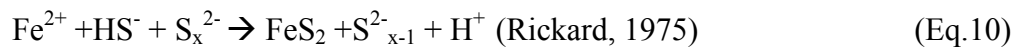
Pore fluid and solid phase chemical analyses of the core SASU 97/3 are presented in Table-1. Pore water sulfate concentrations show linear trend (Fig. 5A) with a gradient of -0.11 mM/cm. The extrapolated depth to the zone of zero sulfate concentration lies at 220.5 cmbsf. AVS could be detected in 12 samples (Table-1) with concentrations ranging from 0.001 to 0.025 wt % of dry sediment. The CRS concentrations vary from 0.07 to 1.64 wt% of dry sediment (Fig. 5B). $\delta^{34}\text{S}_{\text{SO}_4}$ of pore waters (Fig. 5A) increase down depth from $+26.5$ ‰ (VCDT) to $+51.4$ ‰ (VCDT). $\delta^{34}\text{S}_{\text{CRS}}$ (Fig. 5B) increases from -21.9 to -17.4 ‰ (VCDT) down to a depth of 42.5 cmbsf. Below this depth, $\delta^{34}\text{S}_{\text{CRS}}$ show three major peaks with a maximum of $+4.3$ ‰ (VCDT) at a depth of 152.5 cmbsf. Enrichment peaks in sulfur isotope ratios of CRS (demarcated by double sided arrows: Fig. 5B) correspond to the depletions in CRS contents. Concentrations of dithionite extractable iron (Fe_D) decrease exponentially (Fig. 5 C) with depth from 1.92 wt % (at 7.5 cmbsf) to 0.31 wt% (at 162.5 cmbsf). Concentrations of highly reactive iron ($\text{Fe}_{\text{HR}} = \text{Fe}_D + \text{Fe}_{\text{CRS}}$) (Fig. 5C) vary from 0.5 to 2.5 wt% and its trend is similar to that of CRS below 42.5 cmbsf. Above this depth the Fe_{HR} and CRS show broadly opposite trends. Total iron concentration (Fe_T) varies from 5.06 to 7.24 wt% (Avg: 6.24 ± 0.54 wt%) and show a decreasing trend down depth in the core (Table-1). $\text{Fe}_{\text{HR}}/\text{Fe}_T$ ratio ranges from 0.07 to 0.36 (Table-1). OBS/CRS ratio ranges from 0.01 to 5.83 with 57.6% samples having a ratio of more than 1. Depth profiles of OBS and Fe_{HR} contents show overall negative relation (Fig. 6). A negative correlation ($r^2 = -0.65$) is observed between $\delta^{34}\text{S}_{\text{OBS}}$ vs. OBS/CRS ratios (Fig. 7). Total organic carbon concentration (Fig. 8A) content varies from 1.5 to 3.3 wt% (Avg: 2.4 ± 0.03). TOC/TN (Fig. 8B) ranges from 12.4 to 17.3 (Avg: 14.6 ± 1.4). $\delta^{13}\text{C}_{\text{TOC}}$ fluctuates between -21.5 and -24.5 ‰VPDB.

5. Discussion

5.1 Pyrite morphology

Pyrite framboids are microscopic spheroids or subspheroids (Ohfuji and Akai, 2002) of densely packed equidimensional and equimorphic discrete pyrite microcrystals of submicron to ~2 micron size. The number of microcrystals in framboids ranges from 10^3 to 10^4 (Wilkin et al., 1996). The diameter of the framboids (D) increases with increasing microcrystal size (d) (Fig.4). Positive correlation between D and d has also been reported by Ohfuji and Akai, (2002). The average D/d ratio in our study is 12.4 ± 2.9 with 92% samples falling within the D/d of 10 to 20 which is close to the range reported by Ohfuji and Akai (2002). Sawlowicz, (1993) suggested a D/d ratio ~10 for framboids. The variation in D/d ratios is possibly governed by redox conditions, rate of nucleation and growth of initial microcrystals (Ohfuji and Akai, 2002). Framboids with both ordered (cubic close packing or icosahedra) and disordered microcrystal arrangements are known from natural samples (Ohfuji and Akai, 2002; Ohfuji and Rickard, 2005). Framboids do not show bimodal microcrystal size distribution. Framboid formation passes through progressive stages of disordered mackinawite (Fe_{1+x}S) (x ranges from 0.057 to 0.064), ordered mackinawite (Fe_9S_8), greigite (Fe_3S_4) and pyrite (FeS_2). On the other hand, growth of framboid like structures within the template of microbial colonies have been suggested by Maclean et al., (2008) and Gong et al., (2008).

Precipitation of framboidal pyrite suggests a significantly higher nucleation rate than the crystal growth rate (Ohfuji and Rickard, 2005). High nucleation rate needs high supersaturation for pyrite which is facilitated by the presence of intermediate sulfur species, such as S^0 , S_x^{2-} and oxidants like Fe^{3+} and O_2 (Schoonen, 2004). These species are generally expected to be present or produced near the oxic-anoxic interface within the first few centimeters of the sediment or at the chemocline within the water column. Pyritization through polysulfide and iron loss pathways are represented by the equations 10-11.



Syngenetic pyrite framboids precipitating from dysoxic/anoxic water column typically have diameters of 4-6 μm (Suits and Wilkin, 1998; Wilkin et al., 1996). Framboids within this size range are also observed in SASU/97-3 (Fig.4). However, it is difficult to attribute the observed size range to water column anoxia with confidence since these small framboids are mostly confined within foraminifera shells with

limited space which may hinder the growth of larger framboids. In addition, nucleation of a large number of framboids within a confined space (Fig. 3F) possibly limits the size of framboids due to depletion of both sulfide and iron concentrations.

Compared to the porous framboids that originate at or above the sediment water interface, the partial to completely filled framboids suggest precipitation of later generation pyrite crystals either within the inter-microcrystal pore spaces (Fig 3B, C, D and E) or as overgrowth on the pre-existing framboid (Suits and Wilkin, 1998). Filling/overgrowth results in welded and interpenetrating texture (Passier et al., 1997; Wilkin and Barnes, 1997) as observed in figure-3C. Framboids growing within a confined space tend to develop multiple faces due to growth pressure (Fig. 3C and D). The pore spaces in framboids are gradually filled as the amalgamation progresses, which finally results in the formation of massive pyrite spherulites or euhedral pyrite with further overgrowth (Sawlowicz, 1993). Late diagenetic pyritization takes place within the H₂S rich zone, following H₂S pathway (Drobner et al., 1990; Rickard, 1997; Butler et al., 2004) (Eq. 12).



The non-spheroidal aggregates (Fig. 3G, I, J, K, L) of cubo-octahedral pyrite crystal (0.8 to 8.7 μm) are possibly of late diagenetic origin. Passier et al., (1997) reported isolated cubes and octahedras of 2-10 μm and clusters/ irregular aggregates (up to 60 μm) of cubes and octahedras (3-5 μm), filling the foraminifera shells from Mediterranean sapropel and the underlying sediments. The range of crystal sizes in the non-spheroidal aggregates (Fig. 3J and L) suggests a sequential crystallization with decreasing nucleation rate under sulfate limited conditions during late diagenesis. However, the pyrite aggregate could also be a result of late diagenetic replacement of titano magnetite/ hematite particles (Canfield and Berner, 1987). Etch pit formation on titano magnetite grains (Fig. 3H) is an indicator of its dissolution in organic rich marine sediments (Karlin and Levi, 1985). The extent of dissolution depends on the surface area of titano-magnetite grains, concentration of dissolved sulfide and the duration of contact between the titano-magnetite grains and sulfidic pore fluids.

5.2 Pore water chemistry

The pore water sulfate concentrations decreases down depth with a linear gradient. There is a net enrichment of 24.9‰ VCDT of residual pore water sulfate at 157 cmbsf relative to the core top sediment. The increase in sulfur isotope ratios in the residual sulfate is attributed to microbial sulfate reduction (Eqs.1 to 3) which involves preferential breakage of ³²S-¹⁶O bond through enzymatically

catalyzed reactions (Kemp and Thode, 1968; Canfield, 2001, Canfield, 2005) and production of isotopically depleted H₂S. H₂S is eventually removed from the pore water through pyritization, sulfurization of organic compounds and diffusion (Chanton et al., 1987, Ferdelman et al., 1999 and Brüchert et al., 2003) leaving the residual pore water sulfate isotopically enriched. A steady depth-wise enrichment in sulfur isotope ratios ($r^2 = 0.93$) and absence of significant negative perturbations suggest very low contribution of sulfate in the pore water via oxidation of isotopically depleted H₂S during subsampling and pore water extraction. This is further supported by oxygen isotope ratios of pore water sulfate (Supplementary Figure-2 and text).

5.3 Pyritization and role of reactive iron

CRS concentration profile (Fig. 5B) essentially represents the pyritization profile through the sediment column. Depleted S-isotope ratios (-20 to -21‰ VCDT) recorded at the core top are attributed to early diagenetic pyritization close to sediment-water interface where the rate of sulfate diffusion into the sediment pore volume exceeds the rate of sulfate consumption (Jørgensen, 1979; Calvert et al., 1996; Schenau et al., 2002). Since pyritization involves insignificant sulfur isotope fractionation (Price and Shie, 1979), its isotope ratio represents the sulfur isotope composition of pore water HS⁻. A sulfur isotope fractionation of ~40‰ VCDT observed here relative to 21‰ VCDT of the average sea water sulfate (Rees et al., 1978) is within the range of sulfur isotopic fractionation (5 to 46 ‰ VCDT) measured for natural environment and laboratory cultures (Canfield and Teske, 1996; Habicht and Canfield, 1997). Recently, Sim et al.(2011) reported fractionation up to 66 ‰ by sulfate reducing bacteria.

Within the top 42.5 cmbsf of the core, the $\delta^{34}\text{S}_{\text{CRS}}$ oscillates between -15.8 and -21.9 ‰ VCDT. Low CRS content in this zone is associated with high Fe_D content suggest incomplete pyritization of labile iron. Below the depth of 42.5 cm, the CRS wt% and $\delta^{34}\text{S}_{\text{CRS}}$ profiles display opposite trends. The maximum peak value of $\delta^{34}\text{S}_{\text{CRS}}$ recorded here is ± 4.3 ‰ VCDT, i.e., a net enrichment of sulfur isotope ratio of CRS relative to core top by 24.2‰. During sediment burial, the late diagenetic pyrite crystals precipitate with depthwise enrichment in sulfur isotope ratios owing to sulfate limitation in a closed system (Calvert et al., 1996). The overall downward enrichment trend in the S-isotope ratio of CRS is superimposed by repeated depletions corresponding to increase in CRS and Fe_{HR} contents. The depletions in sulfur isotope ratios suggest enhanced pyritization at the sediment water interface coupled with greater flux of highly reactive iron (Schenau et al., 2002). However, incorporation of late

diagenetic pyrite during sediment burial resulted in enrichment of the S-isotope ratio relative to the core top $\delta^{34}\text{S}_{\text{CRS}}$. On the other hand, positive perturbations in the $\delta^{34}\text{S}_{\text{CRS}}$ profile correspond to lows in CRS and Fe_{HR} concentrations. We attribute the low CRS concentrations to reduced Fe_{HR} flux and dominance of relatively less reactive iron ($\text{Fe}_{\text{LR}} = \text{Fe}_{\text{T}} - \text{Fe}_{\text{HR}}$). Slow pyritization of relatively less reactive iron results in the dominance of isotopically enriched pyrite during sediment burial. Various iron bearing minerals which are amenable to pyritization in sediments have a wide range of sulfurization half lives (Canfield et al., 1992; Raiswell and Canfield, 1998, Poulton et al., 2004). The larger proportion of rapidly reactive (low half lives) iron minerals in the sediment leads to enhanced pyritization close to the sediment water interface.

5.4 Sulfurization of organic matter

Sulfurization of organic matter is an important process controlling the abundance of sulfur in sediments (Brüchert and Pratt, 1996, Brüchert, 1998). The sulfurization process is also an important mechanism for the preservation of functionalized organic compounds during early diagenesis (Sinnighe Damsté and de Leeuw, 1990). Intramolecular and intermolecular incorporation of sulfur (Sinnighe Damsté et al., 1989) are the two important pathways of organic matter sulfurization. Compared to assimilatory biosynthesized sulfur (Dinur et al., 1981), organo-sulfur compounds formed by intra- and intermolecular incorporation of sulfur into organic matter during diagenesis are more refractory (Werne et al., 2000) and amenable to preservation. Biosynthesized sulfur has $\delta^{34}\text{S}$ values that are close to the isotopic composition of seawater sulfate owing to nominal fractionation (Goldhaber and Kaplan, 1974). In comparison, early diagenetically formed sulfurized organic matter is characterized by significantly depleted sulfur isotope ratios (Werne et al., 2003). Polysulfide (S_x^{2-}) and elemental sulfur (S^0) are considered as important sulfurizing species during early diagenesis and negligible S-isotope effects occur during incorporation of reduced sulphur into organic matter (Mossmann et al., 1991). Whereas, relative abundance of reactive iron and labile organic compounds influence the concentrations as well as isotopic ratios of diagenetically formed organic bound sulfur (Zaback and Pratt, 1992, Passier et al., 1999). A negative correlation (Fig. 6) between OBS and Fe_{HR} profiles depict influence of iron limitation on sulfurization of organic matter. The extent of organic matter sulfurization in such cases would be governed by availability of labile organic compounds as well as $\text{HS}^- / \text{S}_x^{2-}$ during early diagenesis at the sediment water interface. A negative correlation ($r^2 = -0.65$) between $\delta^{34}\text{S}_{\text{OBS}}$ and OBS/CRS ratios (Fig. 7) suggest limited Fe_{HR} flux and greater availability of labile organic compounds promoting

sulfurization of reactive organic compounds close to sediment water interface resulting in incorporation of isotopically depleted sulfur. Whereas, if reactive iron is readily available compared to labile organic compounds, pyrite formation is believed to be a kinetically favored process at the sediment water interface compared to sulfurization of OM (Gransch and Posthuma, 1973; Hartgers et al., 1997). In this case, sulfurization of organic compounds takes place during late diagenesis, resulting in enriched sulfur isotope ratios of OBS.

5.5 Paleoclimatic / Paleoceanographic implications

The Fe_{HR} trend and Fe_{HR}/Fe_T ratios observed in this study may be linked to paleoclimatic and paleoceanographic processes off the west coast of India. In a typical humid, tropical environment, iron is delivered to the continental margin primarily as riverine, suspended Fe-oxide/hydroxide nano/micro particulates (Raiswell, 2011) derived via chemical weathering of the catchment area (Canfield, 1997; Lamy et al., 2000). High runoff results in increased content of poorly crystalline iron hydroxides/ oxides in the suspended load (Canfield, 1997) which constitutes the Fe_{HR} content of the suspended particulates. Whereas, structurally bound iron in clays, ferromagnesian minerals, titanohematite and titanomagnetite constitute the bulk of unreactive or slowly reactive Fe in sediments (Raiswell and Canfield, 1998). The global average riverine Fe_{HR}/Fe_T ratio is 0.43 ± 0.03 (Poulton and Raiswell, 2002). However, Canfield (1997) reported Fe_{HR}/Fe_T ratios of 0.15 to 0.20 at low runoff and 0.4 to 0.75 at high runoff. The positive correlation between runoff and Fe_{HR}/Fe_T was attributed to increased weathering which produced proportionately more Fe_{HR} at the source. The global average of Fe_{HR}/Fe_T for marginal marine sediments is 0.26 ± 0.09 (Raiswell and Canfield, 1998; Lyons and Severmann, 2006). The drop in Fe_{HR}/Fe_T of marine sediments relative to the riverine average is attributed to the absorption of Fe_{HR} on colloidal precipitates (Benjamin and Honeyman, 1992) at estuaries due to mixing of fresh and saline water (Wen et al., 1999; de Baar and Jong, 2001; Poulton and Raiswell, 2002). Most of colloidal precipitate cannot escape the estuarine mixing zone (de Baar and Jong, 2001) except through resuspension of the bedload (Rao et al., 2011) at the river-sea interface during monsoon. The Fe_{HR} profile (Fig. 5C) shows positive peaks from 1629 ± 36.5 to 1966 ± 3.9 AD. Below the depth of 42.5 cm, Fe_{HR}/Fe_T ratio fluctuates between 0.07 and 0.28 and generally remains lower than the global average (0.26 ± 0.09) for marginal marine sediments. We attribute these fluctuations to variation in Fe_{HR} flux which in turn depends on monsoon driven runoff. The marked increase in Fe_{HR}/Fe_T ratio to 0.36 suggests a rapid and persistent increase in monsoonal intensity.

In the present work we have attempted to link the Fe_{HR} with monsoonal record (since 1871 AD) off west coast, and the total solar irradiance (TSI: Wm^{-2}). The rainfall data is based on quality-controlled monthly records (Sontakke et al., 2008) from a network of rainguages along Konkan-Goa (west coast). The data is taken from the Indian Institute of tropical Meteorology, Pune, India (http://www.tropmet.res.in/static_page.php?page_id=53). The TSI data is based on Steinhilber et al. (2009). TSI is the wavelength-integrated energy of solar radiation received at the top of the earth's atmosphere, associated with sunspot variability and additional solar magnetic features (Fontenla et al., 1999). Covariance of monsoonal intensity and solar activity at multi-decadal or centennial scale is extensively studied and reasonably well established for Indian/Asian monsoon system (Mehta and Lau, 1997; Agnihotri et al., 2002; Agnihotri and Dutta, 2003; Bhattacharya and Narsimha, 2005; Tiwari and Ramesh, 2007; Kurian et al., 2009; Liu et al., 2009; Agnihotri et al., 2011). Agnihotri et al. (2011) observed in phase relationship between TSI and instrumental rainfall record from Konkan-Goa region. In other words, TSI may be used as a reliable proxy for past monsoonal variability in the absence of instrumental rainfall record. In figure- 5 D, we have presented 11 years running average of monsoonal rainfall and TSI data. The peaks and valleys of Fe_{HR} profile are correlated with those of TSI profile using tie-lines. The periods of higher rainfall (high TSI) match closely with the duration of enhanced Fe_{HR} concentrations. The deviations observed are attributed to uncertainty in the age-depth model and other internal factors controlling sediment transportation. Significant fluctuation in monsoonal intensity during the last 450 years, off west, is also displayed by additional proxy like, variations in mean proloculus diameter of benthic foraminifera *Rotalidium annectens* (Nigam et al., 1995; Khare and Nigam, 2006).

Monsoonal fluctuations not only change the runoff, but also influence the intensity of coastal upwelling and marine bioproductivity (Naqvi et al., 2000; Agnihotri et al., 2008, Kurian et al., 2009). Repeated enrichment in phytol and dinosterol concentrations support monsoon induced upwelling of nutrients and enhanced pulses of marine biomass between 1600 and 2000 AD (Kurian et al., 2009). The observed fluctuations in $\delta^{13}C_{TOC}$ and TOC/TN ratios (Fig. 8B) and an overall negative correlation between these parameters may be attributed to rapid changes in the relative contributions of terrestrial and marine biomass to the sediments. Monsoon induced upwelling, marine bioproductivity and enhanced flux of terrestrial biomass leads to coastal hypoxia and production of hydrogen sulfide in the water column (Naqvi et al., 2000) off west coast which may promote syngenetic pyritization and sulfurization of labile organic matter at sediment water interface. We propose that studies on high resolution pyrite grain

size distribution in the sediments as well as in the water column may be carried out to resolve possible contribution of syngenetic pyritization during the brief period of peak hypoxia and HS⁻ enrichment in the water column. It is important to decouple the diagenetic overprinting and primary depositional signals using non-steady state diagenetic modeling to get more insight into high resolution paleoclimatic/oceanographic processes.

6. Conclusion

The present work has highlighted the diagenetic as well as paleoclimatic/ paleoceanographic significance of Fe-C-S geochemistry in a shallow marine depositional system. ²¹⁰Pb_{xs} based age dating has established a chronology of this region which may be tagged with existing paleoclimatic data. Our results show diagenetic partitioning of sulfide into iron sulfide (pyrite) and organosulfur phases. Sulfur partitioning influences the content as well as sulfur stable isotope ratio of OBS. Content of easily reactive iron oxyhydroxide and labile organic compounds in the sediment control the sulfur partitioning pathways. We have reported morphologically distinct early and late diagenetic pyrite clusters. Framboids are the dominant pyrite clusters which formed close to the sediment water interface during early diagenesis. Variable extent of infilling and overgrowth on porous framboids suggest late diagenetic overprinting. Concentrations and $\delta^{34}\text{S}$ profiles of CRS show strikingly opposite trends. The negative $\delta^{34}\text{S}$ perturbation corresponding to enrichment of CRS concentrations has been attributed to pyritization at the sediment water interface coupled with relatively high Fe_{HR} flux. In contrast, the positive $\delta^{34}\text{S}$ perturbation corresponding to low CRS concentration is attributed to dominance of less or slowly reactive iron bearing minerals that resulted in late diagenetic pyritization. We have attempted to link the Fe_{HR} trend, Fe_{HR}/Fe_T ratios with runoff, monsoonal intensity and shallow coastal upwelling. Our inference regarding monsoonal fluctuation, upwelling and productivity variation over the last 378 years gain support from existing paleoclimatic observations from shallow waters off west coast India. Future work will focus on high resolution sampling and age dating in order to collate all the observed parameters into one coherent model.

Acknowledgement

We are grateful to the Director, NIO for allowing us to carry out this investigation. Thanks are due to A.V. Mudholkar, M. Shyamprasad, V.D. Khedeker and M. Caesar for the help in availing SEM-EDX and XRF facilities at NIO. Research fellowship from VNJCT to A. Peketi is sincerely acknowledged. We express sincere gratitude to Dileep Kumar, R. Agnihotri and P.C. Rao and the reviewers for valuable comments. The work was funded by OLP0012.

References

- Agnihotri, R., Dutta, K., Soon, W., 2011. Temporal derivative of total solar irradiance and anomalous Indian summer monsoon: An empirical evidence for a Sun-climate connection. *J. Atmos. Solar-Terrstris Phys.* 73, 1980-1987.
- Agnihotri, R., Dutta, K., 2003. Centennial scale variations in monsoonal rainfall (Indian, east equatorial and Chinese monsoons): Manifestation of solar variability. *Current Sci.* 85, 459-463.
- Agnihotri, R., Dutta, K., Bhushan, R., Somayajulu, B.L.K., 2002. Evidence for solar forcing on the Indian monsoon during the last millennium. *Earth and Planetary Science Letters* 198, 521-527.
- Agnihotri, R., Kurian, S., Fernandes, M., Reshma, K., D'Souza, W., Naqvi, S.W. A., 2008. Variability of subsurface denitrification and surface productivity in the coastal eastern Arabian Sea over the past seven centuries. *The Holocene* 18, 755-764.
- Benjamin, M.M and Honeyman, B.D., 1992. Trace metals, in Butcher, S.S., Charlson, R.J., Orians, G.H., Wolfe, G.E. (Eds.), *Global Biogeochemical Cycle*, Academic Press limited, London, pp. 317-346.
- Berner, R.A., 1978. Sulfate reduction and the rate of deposition of marine sediments. *Earth and Planetary Science Letters* 37, 492-498.
- Bhattacharyya, S., Narsimha, R., 2005. Possible association between Indian monsoon rainfall and solar activity. *Geophys. Res. Lett.*, 32, L05813.
- Bhalla, U., Basavaiah, N., Deenadayalan, K., Borole, D.V., Mohite, R.D., 2011. Onset of industrial pollution recorded in Mumbai mudflat sediments, using integrated magnetic, Chemical, ^{210}Pb dating, and microscopic methods. *Environmental Science and Technology* 45, 2011, 686-692.
- Boetius, A., Ravenschlag, K., Schubert, C.J., Rickert, D., Widdel, F., Giesecke, A., Amann, R., Jørgensen, B.B., Witte, U., Pfannkuche, O., 2000. A marine microbial consortium apparently mediating anaerobic oxidation of methane. *Nature* 407, 623– 626.
- Brüchert, V., 2004. Physiological and ecological aspects of sulfur isotope fractionation during bacterial sulfate reduction. Amend, J.P., Edwards K.J. and Lyons T.W.(Eds.), *Sulfur Biogeochemistry—Past and Present*. GSA Special Paper 379, pp. 1–16.
- Brüchert, V., 1998. Early diagenesis of sulfur in estuarine sediments: The role of sedimentary humic and fulvic acids. *Geochimica et Cosmochimica Acta* 62, 1567-1586.
- Brüchert, V., Jørgensen B.B., Neumann, K., Riechmann, D., Schlösser, M., Schulz H., 2003. Regulation of bacterial sulfate reduction and hydrogen sulfide fluxes in the central Namibian coastal upwelling zone. *Geochimica et Cosmochimica Acta* 67, 4505-4518.
- Brüchert, V., Pratt, L.M., 1996. Contemporaneous early diagenetic formation of organic and inorganic sulfur in estuarine sediments from St. Andrew Bay, Florida, USA. *Geochimica et Cosmochimica Acta* 60, 2325-2332.

- Butler, I.B., Bftcherb, M.E., Rickarda, D. & Oldroyda, A., 2004. Sulfur isotope partitioning during experimental formation of pyrite via the polysulfide and hydrogen sulfide pathways: implications for the interpretation of sedimentary and hydrothermal pyrite isotope records. *Earth and Planetary Science Letters* 228, 495– 509.
- Calvert, S., Thode, H., Yeung, D., Karlin, R., 1996. A stable isotope study of pyrite formation in the Late Pleistocene and Holocene sediments of the Black Sea. *Geochimica et Cosmochimica Acta* 60, 1261-1270.
- Canfield, D.E., 1989. Sulfate reduction and oxic respiration in marine sediments: implications for organic carbon preservation in euxinic environments. *Deep Sea Research Part A. Oceanographic Research Papers*, 36, 121-138.
- Canfield, D.E., 1997. The geochemistry of river particulates from the continental USA: Major elements. *Geochimica et Cosmochimica Acta* 61, 3349-3365.
- Canfield, D.E., 2001. Biogeochemistry of sulfur isotopes. *Reviews in Mineralogy and Geochemistry* 43, 607-636.
- Canfield, D.E., 2005. The sulfur cycle. *Advances in Marine Biology* 48, 313-381.
- Canfield, D.E., Berner, R., 1987. Dissolution and pyritization of magnetite in anoxic marine sediments. *Geochimica et Cosmochimica Acta* 51, 645-659.
- Canfield, D.E., Olesen, C.A., Cox, R.P., 2006. Temperature and its control of isotope fractionation by a sulfate-reducing bacterium. *Geochimica et Cosmochimica Acta* 70, 548-561.
- Canfield, D.E., Raiswell R. and Bottrell, S., 1992. The reactivity of sedimentary iron minerals toward sulfide. *American Journal Science*, 292, 659–683.
- Canfield, D., Raiswell, R., Westrich, J., Christopher M. Reaves, C.M., Berner, R.A., 1986. The use of chromium reduction in the analysis of reduced inorganic sulphur in sediments and shales. *Chemical Geology*, 54, 149-155.
- Canfield, D.E., Teske, A., 1996. Late Proterozoic rise in atmospheric oxygen concentration inferred from phylogenetic and sulphur-isotope studies. *Nature* 382, 127–132.
- Chanton, J., Martens, C., Goldhaber, M., 1987. Biogeochemical cycling in an organic-rich coastal marine basin. Sulfur mass balance, oxygen uptake and sulfide retention. *Geochimica et Cosmochimica Acta* 51, 1187-1199.
- Claypool, G., 2004. Ventilation of marine sediments indicated by depth profiles of pore water sulfate and $\delta^{34}\text{S}$. *The Geochemical Society Special Publications* 9, 59-65.
- de Baar, H.J.W., de Jong, J.T.M., 2001. Distribution, sources and sinks of iron in seawater. In: Turner, D.R., Hunter, K.H. (Eds.), *The Biogeochemistry of Iron in Seawater*, IUPAC Series on Analytical and Physical Chemistry of Environmental Systems, 7, 123–253.

- Detmers, J., Bruchert, V., Habicht, K., Kuever, J., 2001. Diversity of sulfur isotope fractionations by sulfate-reducing prokaryotes. *Applied and Environmental Microbiology* 67, 888-894.
- Dickin, A.P., 1995. Radiogenic isotope geology. Cambridge University Press. pp 490.
- Dinur, D., Spiro, B., Aizenshtat, Z., 1981. The distribution and isotopic composition of sulfur in organic-rich sedimentary rocks. *Chemical Geology* 31, 37-51.
- Drobner, E., Huber, H., Wächtershäuser, G., Rose, D., Stetter, K., 1990. Pyrite formation linked with hydrogen evolution under anaerobic conditions. *Nature* 346, 742-744.
- Ferdelman, T.G., Fossing, H., Neumann, K., Schulz, H.D., 1999. Sulfate Reduction in surface sediments of the southeast Atlantic continental margin between 15 38'S and 27 57'S (Angola and Namibia). *Limnology and Oceanography* 44, 650–661.
- Fontenla, J., White, O.R., Fox, P.A., Avrett, E.H., Kurucz, R.L., 1999. Calculation of solar irradiances. I. Synthesis of the solar spectrum. *The Astrophysical Journal* 518, 480-499.
- Gelinas, Y., Baldock, J., Hedges, J., 2001. Organic carbon composition of marine sediments: Effect of oxygen exposure on oil generation potential. *Science* 294, 145-148.
- Gieskes, J.M., Gamo, T., Brumsack, H., 1991. Chemical methods for interstitial water analysis aboard *JOIDES Resolution*. Ocean Drilling Program Technical Note 15.
- Goldhaber, M., 2003. Sulfur-rich sediments. In: Heinrich D. Holland and Karl K. Turekian (Eds.), *Treatise on Geochemistry*, vol. 7, pp. 257-288.
- Goldhaber, M., Kaplan, I., 1974. The sulfur cycle. In: Goldberg, E (Ed.) *The Sea*. 5, 569-655.
- Goldhaber, M., Kaplan, I., 1975. Controls and consequences of sulfate reduction rates in recent marine sediments. *Soil Science* 119, 42-55.
- Gong, Y.M., Shi, G.R., Weldon, E.A., Du, Y.S., Xu, R., 2008. Pyrite framboids interpreted as microbial colonies within the Permian Zoophycos spreiten from southeastern Australia. *Geological Magazine* 145, 95–103.
- Gransch, J.A., and Posthuma, J., 1973. On the origin of sulphur in crudes. In: Tissot, B., Bienner, F., (Eds.), *Advances in Organic Geochemistry*, Technip, Paris, pp. 727–739.
- Habicht, K., Canfield, D., 1997. Sulfur isotope fractionation during bacterial sulfate reduction in organic-rich sediments. *Geochimica et Cosmochimica Acta* 61, 5351-5361.
- Hansen, M.H., Ingvorsen, K., Jørgensen, B.B., 1978. Mechanisms of hydrogen sulfide release from coastal marine sediments to the atmosphere. *Limnology and Oceanography* 23, 68-76.
- Harrison, A.G., Thode, H.G., 1958. Mechanism of the bacterial reduction of sulfate from isotopic fractionation studies. *Transaction Faraday Society* 54, 84-92.

- Hartgers, W.A., Lopez, J.F., Sinnighé-Damste, J.S., Reiss, C., Maxwell, J.R., Grimalt, J.O., 1997. Sulfur-binding in recent environments: II. Speciation of sulfur and iron and implications for the occurrence of organo-sulfur compounds. *Geochimica et Cosmochimica Acta* 61, 4769-4788.
- Hashimi, N., Nigam, R., Nair, R., Rajagopalan, G., 1995. Holocene sea level fluctuations on western Indian continental margin: An update. *Journal of the Geological Society of India* 46, 157-162.
- Hedges, J., Keil, R., 1995. Sedimentary organic matter preservation: an assessment and speculative synthesis. *Marine Chemistry* 49, 81-115.
- Hoehler, T.M. and Alperin, M.J., 1996. Anaerobic methane oxidation by methanogen-sulfate reducer consortium: Geochemical evidence and biochemical considerations, In: Lindstrom, M.E., Tabita, F.R. (Eds.), *Microbial Growth on C₁ compounds*, Elsevier, pp. 53–75.
- Jørgensen, B., 1979. A theoretical model of the stable sulfur isotope distribution in marine sediments. *Geochimica et Cosmochimica Acta* 43, 363-374.
- Jørgensen, B., 1990. The sulfur cycle of freshwater sediments: Role of thiosulfate. *Limnology and Oceanography*: 1329-1342.
- Jørgensen, B., 1982. Mineralization of organic matter in the sea bed—the role of sulphate reduction. *Nature* 296, 643-645.
- Karisiddaiah, S., Veerayya, M., 1996. Potential distribution of subsurface methane in the sediments of the eastern Arabian Sea and its possible implications. *Journal of Geophysical Research* 101, 25887-25895.
- Karisiddaiah, S., Veerayya, M., Vora, K., 2002. Seismic and sequence stratigraphy of the central western continental margin of India: late-Quaternary evolution. *Marine Geology* 192, 335-353.
- Karisiddaiah, S., Veerayya, M., Vora, K., Wagle, B., 1993. Gas-charged sediments on the inner continental shelf off western India. *Marine Geology* 110, 143-152.
- Karlin, R., Levi, S., 1985. Geochemical and sedimentological control of the magnetic properties of hemipelagic sediments. *Journal of Geophysical Research*, 90, 10373-10392.
- Kasten, S., Jørgensen, B.B., 2000. Sulfate Reduction in Marine Sediments. *Marine geochemistry*: 263-275.
- Kemp, A., Thode, H., 1968. The mechanism of the bacterial reduction of sulphate and of sulphite from isotope fractionation studies. *Geochimica et Cosmochimica Acta* 32, 71-91.
- Khare, N., Nigam, R., 2006. Can the possibility of some linkage of monsoonal precipitation with solar variability be ignored? Indications from foraminiferal proxy records. *Current Science* 90, 1685-1688.
- Krishnaswami, S., Lal, D., 1978. Radionuclide limnology. In: Lerman, A. (Ed.), *Lakes Chemistry, Geology and Physics*. Springer-Verlag, NY, pp. 153–177

- Kristensen, E., 2000. Organic matter diagenesis at the oxic/anoxic interface in coastal marine sediments, with emphasis on the role of burrowing animals. *Hydrobiologia* 426, 1-24.
- Kump, L., Garrels, R., 1986. Modeling atmospheric O₂ in the global sedimentary redox cycle. *American Journal of Science* 286, 337-360.
- Kurian, S., Agnihotri, R., Borole, D.V., Naqvi, S.W.A., Ferreira, A.M. and Vale, C., 2009. Possible solar control on primary production along the Indian west coast on decadal to centennial timescale. *Journal of Quaternary Science* 24, 109-116.
- Lamy, F., Klump, J., Hebbeln, D., Wefer, G., 2000. Late quaternary rapid climate change in northern Chile. *Terra Nova* 12, 8-13.
- Liu, X., Dong, H., Yang, X., Herzschuh, U., Zhang, E., Stuut, Jan-Bernard W., Wang, Y., 2009. Late Holocene forcing of the Asian winter and summer monsoon as evidenced by proxy records from the northern Qinghai-Tibetan Plateau. *Earth and Planetary Science Letters*, 280, 276-284.
- Lyons, T.W., Severmann, S., 2006. A critical look at iron paleoredox proxies: New insights from modern euxinic marine basins. *Geochimica et Cosmochimica Acta* 70, 5698-5722.
- Maclean, L.C.W., Tyliszczak, T., Gilbert, P., Zhou, D., Pray, T.J., Onstott, T.C., Southam, G., 2008. A high resolution chemical and structural study of framboidal pyrite formed within a low temperature bacterial biofilm. *Geobiology* 6, 471-480.
- Madigan, M., Martinko, J., and Parker, J., 2000. *Biology of Microorganisms*. Prentice-Hall, New Jersey.
- Mazumdar, A., Peketi, A., Dewangan, P., Badesab, F., Ramprasad, T., Raman, M.V., Patil, D.J., Daya, A., 2009. Shallow gas charged sediments off the Indian west coast: Genesis and distribution. *Marine Geology* 267, 71-85.
- Mazumdar, A., Strauss, H., 2006. Sulfur and strontium isotopic compositions of carbonate and evaporite rocks from the late Neoproterozoic–early Cambrian Bilara Group (Nagaur-Ganganagar Basin, India): Constraints on intrabasinal correlation and global sulfur cycle. *Precambrian Research* 149, 217–230.
- Megonigal, J., Hines, M., Visscher, P., 2003. Anaerobic metabolism: linkages to trace gases and aerobic processes. *Treatise on geochemistry*. In: Heinrich D. Holland, H.D., Turekian, K.K. (Eds.), 8, 317-424.
- Mehra, O.P., and Jackson, M.L., 1960. Iron oxide removal from soils and clays by a dithionate-citrate system buffered with sodium bicarbonate. In: Swineford, A. (Ed.), *Clays and clay minerals, proceedings of the Seventh National Conference*: London. pp. 317-327.
- Mehta, V., Lau, K. M., 1997. Influence of solar irradiance on the Indian monsoon-ENSO relationship at decadal-multidecadal scales. *Geophysical Research Letters*, 24, 159-162.

- Mossmann, J., Aplin, A., Curtis, C., Coleman, M., 1991. Geochemistry of inorganic and organic sulphur in organic-rich sediments from the Peru Margin. *Geochimica et Cosmochimica Acta* 55, 3581-3595.
- Nair, R.R., Hashimi, N.H., Kidwai, R.M., Guptha, M.V.S., Paropkari, A.L., Ambre, N. V., Muralinath, A.S., Mascarenhas, A., D'Costa, G.P., 1978. Topography and sediments of the western continental shelf of India-Vengurla to Mangalore. *Indian Journal Marine of Science* 7, 224-230.
- Nair, R., Pylee, A., 1969. Size distribution and carbonate content of the sediments of the western shelf of India. *Bulletine of National Institute of Sciences of India* 38, 411-420.
- Naqvi, S.W.A., Jayakumar, D.A., Narvekar, P.V., Naik, H., Sarma, V.V.S.S., DeSouza, W., Joseph, S., George, M.D., 2000. Increased marine production of N₂O due to intensifying anoxia on the Indian continental shelf. *Nature* 408, 346-349.
- Naqvi, S.W.A., Naik, H., Jayakumar, D.A., Shailaja, M. S., Narvekar, R. V., 2006. Seasonal oxygen deficiency over the western continental shelf of India, In: Neretin, L., (Ed.), *Past and Present Water Column Anoxia*. NATO Science Series, IV. Earth and Environmental Sciences 64, Springer., 195-224.
- Nigam, R., Khare, N., Nair, R., 1995. Foraminiferal evidences for 77-year cycles of droughts in India and its possible modulation by the gleissberg solar cycle. *Journal of Coastal Research* 11, 1099-1107.
- Ohfuji, H., Akai, J., 2002. Icosahedral domain structure of framboidal pyrite. *American Mineralogist* 87, 176-180.
- Ohfuji, H., Rickard, D., 2005. Experimental syntheses of framboids--a review. *Earth-Science Reviews* 71, 147-170.
- Orphan, V.J., House, C.H., Hinrichs, K.U., McKeegan, K.D., DeLong, E.F., 2001. Methane-consuming archaea revealed by directly coupled isotopic and phylogenetic analysis. *Science* 293, 484-487.
- Passier, H., Middelburg, J., De Lange, G., Böttcher, M., 1997. Pyrite contents, microtextures, and sulfur isotopes in relation to formation of the youngest eastern Mediterranean sapropel. *Geology* 25, 519-522.
- Passier, H., Middelburg, J., de Lange, G., Böttcher, M., 1999. Modes of sapropel formation in the eastern Mediterranean: some constraints based on pyrite properties. *Marine Geology* 153, 199-219.
- Poulton, S., Krom, M., Raiswell, R., 2004. A revised scheme for the reactivity of iron (oxyhydr) oxide minerals towards dissolved sulfide. *Geochimica et Cosmochimica Acta*, 68, 3703-3715.
- Poulton, S., Raiswell, R., 2002. The low-temperature geochemical cycle of iron: from continental fluxes to marine sediment deposition. *American Journal of Science* 302, 774-805.

- Price, F., Shieh, Y., 1979. Fractionation of sulfur isotopes during laboratory synthesis of pyrite at low temperatures. *Chemical Geology* 27, 245-253.
- Raiswell, R., Canfield, D., 1998. Sources of iron for pyrite formation in marine sediments. *American Journal of Science* 298, 219-245.
- Raiswell, R., 2011. Iron Transport from the Continents to the Open Ocean: The Aging–Rejuvenation Cycle. *Elements* 7, 101-106.
- Rao, V.P., Shynu, R., Kessarkar, P.M., Sundar, D., Michael, G.S., Narvekar, T., Blossom, V., Mehra, P., 2011. Suspended sediment dynamics on a seasonal scale in the Mandovi and Zuari estuaries, central west coast of India. *Estuarine, Coastal and Shelf Science* 91, 78-86.
- Rao, V.P., Wagle, B., 1997. Geomorphology and surficial geology of the western continental shelf and slope of India: A review. *Current Science* 73, 330-350.
- Rees, C., Jenkins, W., Monster, J., 1978. The sulphur isotopic composition of ocean water sulphate. *Geochimica et Cosmochimica Acta* 42, 377-381.
- Rickard, D., 1997. Kinetics of pyrite formation by the H₂S oxidation of iron (II) monosulfide in aqueous solutions between 25 and 125 C: The rate equation. *Geochimica et Cosmochimica Acta* 61, 115-134.
- Rickard, D., 1975. Kinetics and mechanism of pyrite formation at low temperatures. *American Journal of Science* 275, 636-652.
- Roychoudhury, A.N., Kostka, J.E., Van Cappellen, P., 2003. Pyritization: a palaeoenvironmental and redox proxy reevaluated. *Estuarine, Coastal and Shelf Science*, 57, 1183-1193.
- Sawlowicz, Z., 1993. Pyrite framboids and their development: a new conceptual mechanism. *Geologische Rundschau* 82, 148-156.
- Schenau, S., Passier, H., Reichart, G., De Lange, G., 2002. Sedimentary pyrite formation in the Arabian Sea. *Marine Geology* 185, 393-402.
- Schoonen, M.A.A., 2004, Mechanisms of sedimentary pyrite formation. In *Sulfur biogeochemistry—Past and present*. In: Amend, J.P., Edwards, K.J., Lyons T.W. (Eds.), *Geological Society of America Special Paper* 379, Boulder, Colorado, pp.117–134.
- Sharma, P., Borole, D.V, Zingde, M.D., 1994. ²¹⁰Pb based trace element fluxes in the near shore and estuarine sediments off Bombay, India. *Marine Chemistry*, 47, 227-241.
- Shen, Y., Buick, R., 2004. The antiquity of microbial sulfate reduction. *Earth-Science Reviews* 64, 243-272.
- Siddiquie, H., Rao, D.G., Vora, K., Topgi, R., 1981. Acoustic masking in sediments due to gases on the western continental shelf of India. *Marine Geology* 39, 27-37.

- Sim, M. S., Bosak, T. and Ono, S., 2011. Large sulfur isotope fractionation does not require disproportionation. *Science* 333, 74-77.
- Sinninghe Damsté, J., Eglinton, T., De Leeuw, J., Schenck, P., 1989. Organic sulphur in macromolecular sedimentary organic matter: I. Structure and origin of sulphur-containing moieties in kerogen, asphaltenes and coal as revealed by flash pyrolysis. *Geochimica et Cosmochimica Acta* 53, 873-889.
- Sinninghe Damsté, J.S., De Leeuw, J.W., 1990. Analysis, structure and geochemical significance of organically-bound sulphur in the geosphere: state of the art and future research. *Organic Geochemistry* 16, 1077-1101.
- Skyring, G., 1987. Sulfate reduction in coastal ecosystems. *Geomicrobiology Journal* 5, 295-374.
- Sontakke, N.A. Singh, N., Singh, H.N., 2008. Instrumental period rainfall series of the Indian region (AD 1813–2005): revised reconstruction. *The Holocene* 18, 1055–1066.
- Steinhilber, F., Beer, J., Frönlich, C., 2009. Total solar irradiance during the Holocen. *Geophys. Res. Lett.*, 36,
- Strauss, H., 1997. The isotopic composition of sedimentary sulfur through time. *Palaeogeography, Palaeoclimatology, Palaeoecology* 132, 97-118.
- Suits, N., Wilkin, R., 1998. Pyrite formation in the water column and sediments of a meromictic lake. *Geology* 26, 1099-1102.
- Sweeney, R., Kaplan, I., 1980. Diagenetic sulfate reduction in marine sediments. *Marine Chemistry* 9, 165-174.
- Tiwari, M., Ramesh, R., 2007. Indian Monsoon-Solar connection. In: *Proceeding of 12th ISMAS Symposium cum Workshop on Mass Spectrometry, Donapaula, Goa, India*
- Trust, B., Fry, B., 1992. Stable sulphur isotopes in plants: a review. *Plant, Cell & Environment* 15, 1105-1110.
- Tuttle, M.L., Goldhaber, M.B., Williamson, D.L., 1986. An analytical scheme for determining forms of sulphur in oil shales and associated rocks. *Talanta* 33, 953-61.
- Valentine, D.L., 2002. Biogeochemistry and microbial ecology of methane oxidation in anoxic environments: a review. *Antonie Van Leeuwenhoek* 81, 271-282.
- Wagle, B., Vora, K., Karisiddaiah, S., Veerayya, M., Almeida, F., 1994. Holocene submarine terraces on the western continental shelf of India; Implications for sea-level changes. *Marine Geology* 117, 207-225.
- Wen, L.S., Santschi, P., Gill, G., Paternostro, C., 1999. Estuarine trace metal distributions in Galveston Bay: importance of colloidal forms in the speciation of the dissolved phase. *Marine Chemistry* 63, 185-212.

- Werne, J.P., Hollander, D.J., Behrens, A., Schaeffer, P., Albrecht, P., Sinninghe Damsté, J.S.S., 2000. Timing of early diagenetic sulfurization of organic matter: a precursor–product relationship in Holocene sediments of the anoxic Cariaco Basin, Venezuela. *Geochimica et Cosmochimica Acta* 64, 1741–1881.
- Werne, J., Lyons, T., Hollander, D., Formolo, M., Sinninghe Damsté, J., 2003. Reduced sulfur in euxinic sediments of the Cariaco Basin: sulfur isotope constraints on organic sulfur formation. *Chemical Geology* 195, 159-179.
- Westrich, J., Berner, R., 1988. The effect of temperature on rates of sulfate reduction in marine sediments. *Geomicrobiology Journal* 6, 99-117.
- Wilkin, R., Barnes, H., 1996. Pyrite formation by reactions of iron monosulfides with dissolved inorganic and organic sulfur species. *Geochimica et Cosmochimica Acta* 60, 4167-4179.
- Wilkin, R., Barnes, H., 1997. Formation processes of framboidal pyrite. *Geochimica et Cosmochimica Acta* 61, 323-339.
- Wilkin, R., Barnes, H., Brantley, S., 1996. The size distribution of framboidal pyrite in modern sediments: An indicator of redox conditions. *Geochimica et Cosmochimica Acta* 60, 3897-3912.
- Zaback, D., Pratt, L., 1992. Isotopic composition and speciation of sulfur in the Miocene Monterey Formation: Reevaluation of sulfur reactions during early diagenesis in marine environments. *Geochimica et Cosmochimica Acta* 56, 763-774.
- Zopfi J., Ferdelman TG., Fossing H., 2004. Distribution and fate of sulfur intermediates - sulfite, tetrathionate, thiosulfate, and elemental sulfur - in marine sediments. In: Amend, J.P., Edwards, K.J., Lyons, T.W. (Eds.) *Sulfur Biogeochemistry - past and present*. Geological Society of America Special Paper 379, pp. 97-116.
- Böttcher, M.E., Bernasconi, S.M., Brumsack, H.J., 1999. Carbon, sulphur, and oxygen isotope geochemistry of interstitial waters from western Mediterranean. In: Zahn, R., Cornas., M.C., Klaus, A. (Eds.), *Proceedings of the Ocean Drilling Program, Scientific Results*, pp. 413–421.
- Lloyd, R.M., 1967. Oxygen-18 composition of ocean sulfate. *Science* 156, 425–428.
- Turchyn, A.V., Sivan . O. and Schrag, D.P. ., 2006, Oxygen isotopic composition of sulfate in deep sea pore fluid: evidence for rapid sulfur cycling. *Geobiology*, **4** (2006), pp. 191–201.

Figure and Table Captions

Figure-1. Map showing coring location (Sasu 97/3) off Cabo-de-rama (Goa, India). The square in the inset shows study area.

Figure-2. Down core profile of $^{210}\text{Pb}_{\text{excess}}$.

Figure-3. (A) Pyrite framboid with octahedral microcrystals. (B) Pyrite framboid with interpenetrating microcrystals and infilled pore spaces (arrow) with late diagenetic pyrite. (C) Pyrite framboids with late diagenetic infilling. Framboids are non-spherical (black arrow) due to growth pressure within the confined space of siliceous tests. Isolated single octahedral pyrite crystals (white arrow) are present in the inter-framboidal pore space. (D) Deformed multiple pyrite framboids with partial infilling (arrow). (E) Pyrite framboids with interpenetrating microcrystals (white arrow) and infilled pore spaces (black arrows) with late diagenetic pyrite. (F) Multiple pyrite framboids. (G) Megafamboidal pyrite with large cubo-octahedral crystals, (H) Etched titano-magnetite crystal. (I-L) Large aggregates of cubo-octahedral pyrites with variable crystal sizes.

Figure-4. Cross plot between pyrite framboid (D) and microcrystal (d) diameters. The dotted lines represent different D/d ratios.

Figure-5. Depth profile of (A) pore water sulfate concentrations and $\delta^{34}\text{S}_{\text{SO}_4}$, (B) CRS (wt%) and $\delta^{34}\text{S}_{\text{CRS}}$. The double sided arrows show the zones of negative correlation. (C) Fe_D and Fe_{HR} concentrations. (D) Composite plot of monsoonal rainfall (1870-2003 AD) and TSI data (1625-2002). The sources of data are mentioned in the text. The dotted lines are tie lines joining similar ages.

Figure-6. Depth profiles of Fe_{HR} (wt%) and OBS (wt%) .

Figure-7. Cross plots between OBS/CRS ratio and $\delta^{34}\text{S}_{\text{OBS}}$. Data points within the box are excluded from regression line.

Figure-8. Depth profiles of (A) TOC (wt%), (B) TOC/TN and $\delta^{13}\text{C}_{\text{TOC}}$,

Table-1. Data on pore water and solid phase analyses.

Supplementary Figure-1. MSCL based porosity data.

Supplementary Figure-2. (A) cross plot of sulfur and oxygen isotope ratios of pore water sulfate in SASU 97/3 sediment core. (B) Figure from Böttcher, et al, 1999

Supplementary Figure-1: MSCL based porosity data.

Supplementary Figure2:

Oxygen isotope ratio of the pore water sulfate was measured to assess the possible influence of artifact sulfate produced via (hydrogen) sulfide oxidation on total sulfate concentration and S-isotope ratios during sample handling. $\delta^{18}\text{O}$ of sea water sulfate is 9.3‰ VSMOW. During burial of the pore waters the oxygen isotope ratio of residual sulfate gets enriched with depth due to sulfate reduction (Botcher et al., 1999, Turchyn et al., 2006). The plot of $\delta^{34}\text{S}$ vs $\delta^{18}\text{O}$ of residual pore waters (Suppl Fig.1A) in Sasu 97/3 shows a covariance in S and oxygen isotope ratios upto $\delta^{18}\text{O}$ of 22.2‰ VSMOW corresponding to $\delta^{34}\text{S}$ of 40.5‰ VCDT. Further enrichment in sulfur ratio shows saturation of $\delta^{18}\text{O}$ at ~23‰ VSMOW.

This trend is similar to the observations of Bottcher et al (1999) and Turchyn et al.(2006) and represents the sulfur and oxygen isotope evolution of residual pore water sulfate during burial. $\delta^{18}\text{O}$ of atmospheric oxygen and sea water is +23.5‰ and +9.3‰ VSMOW respectively. Oxidation of hydrogen sulfide by atmospheric oxygen to sulfate results in a fractionation of ~ -8.76 ‰ (Lloyd, 1967) for sulfate oxygen isotope. The double side dotted line in the suppl. figure 1A shows the possible range of S and oxygen isotope ratios of artifact sulfate produced via oxidation of hydrogen sulfide in the studied core. The proposed range for sulfur isotope ratios is based on the $\delta^{34}\text{S}_{\text{CRS}}$. It is apparent from the figure that the sulfur isotope ratios reported in the study are least influenced by artifact sulfate.

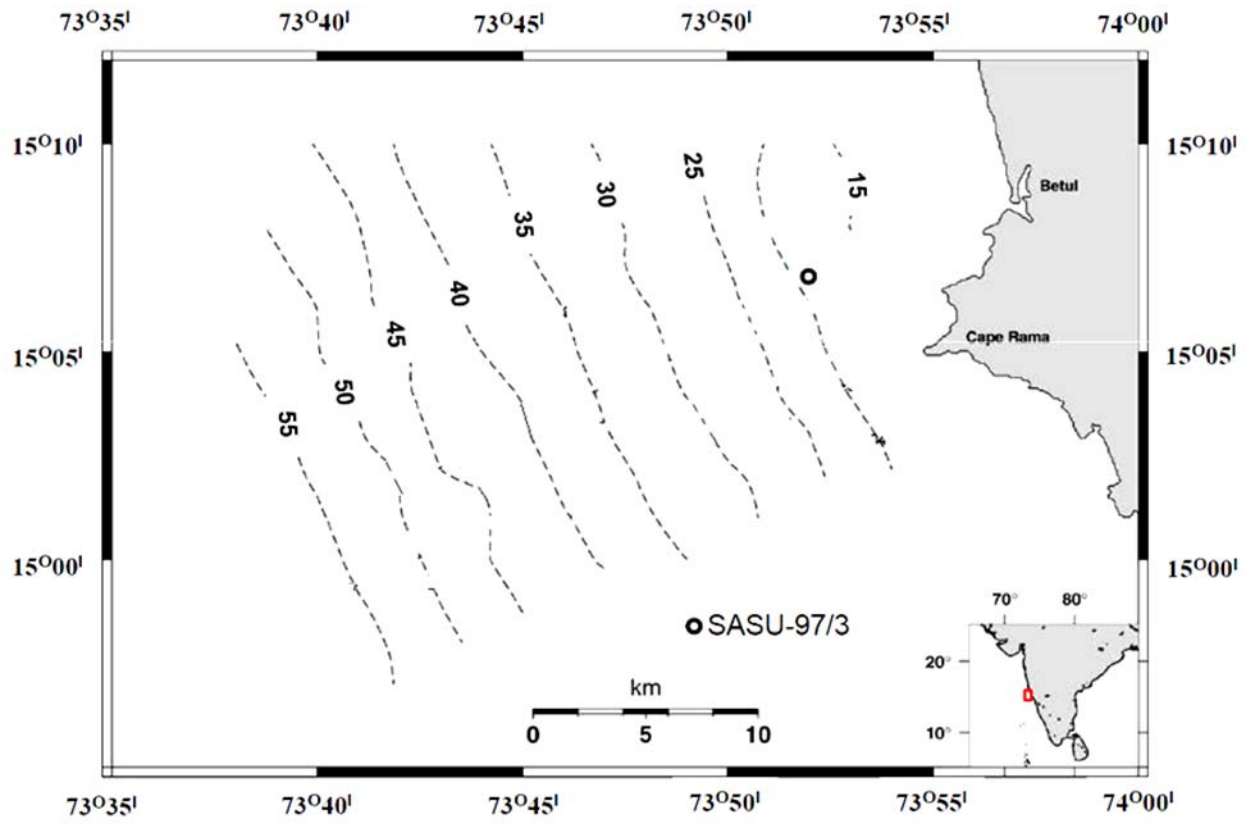


Figure-1

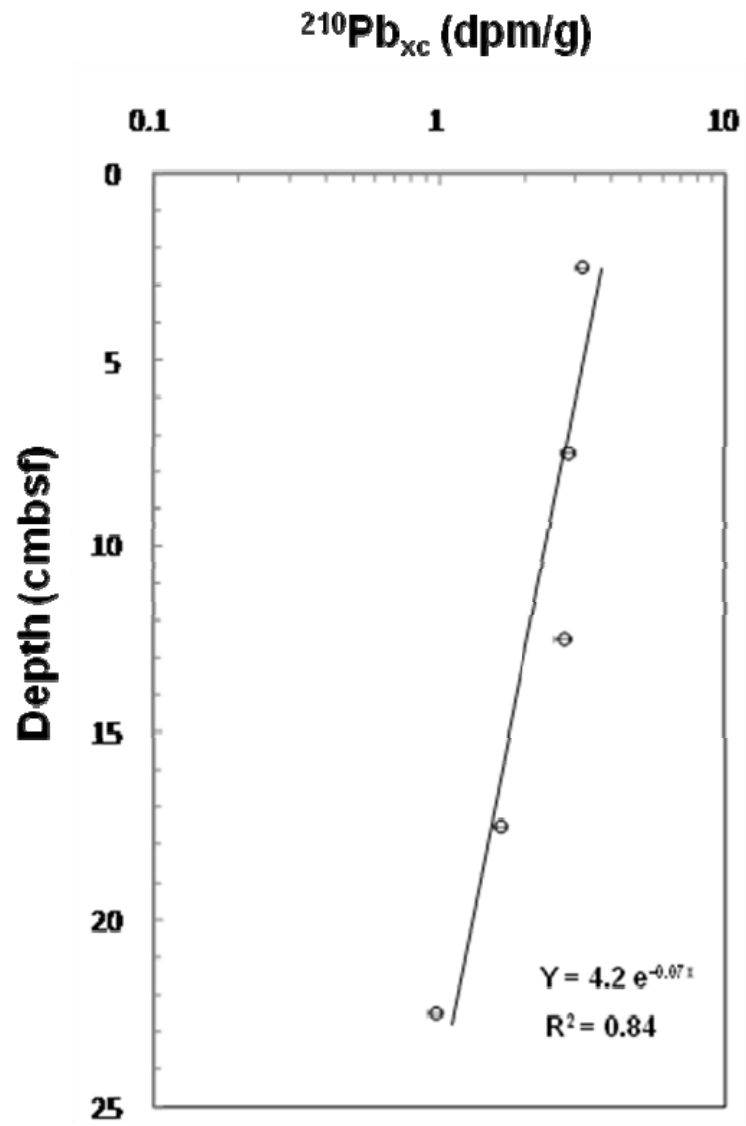


Fig. 2

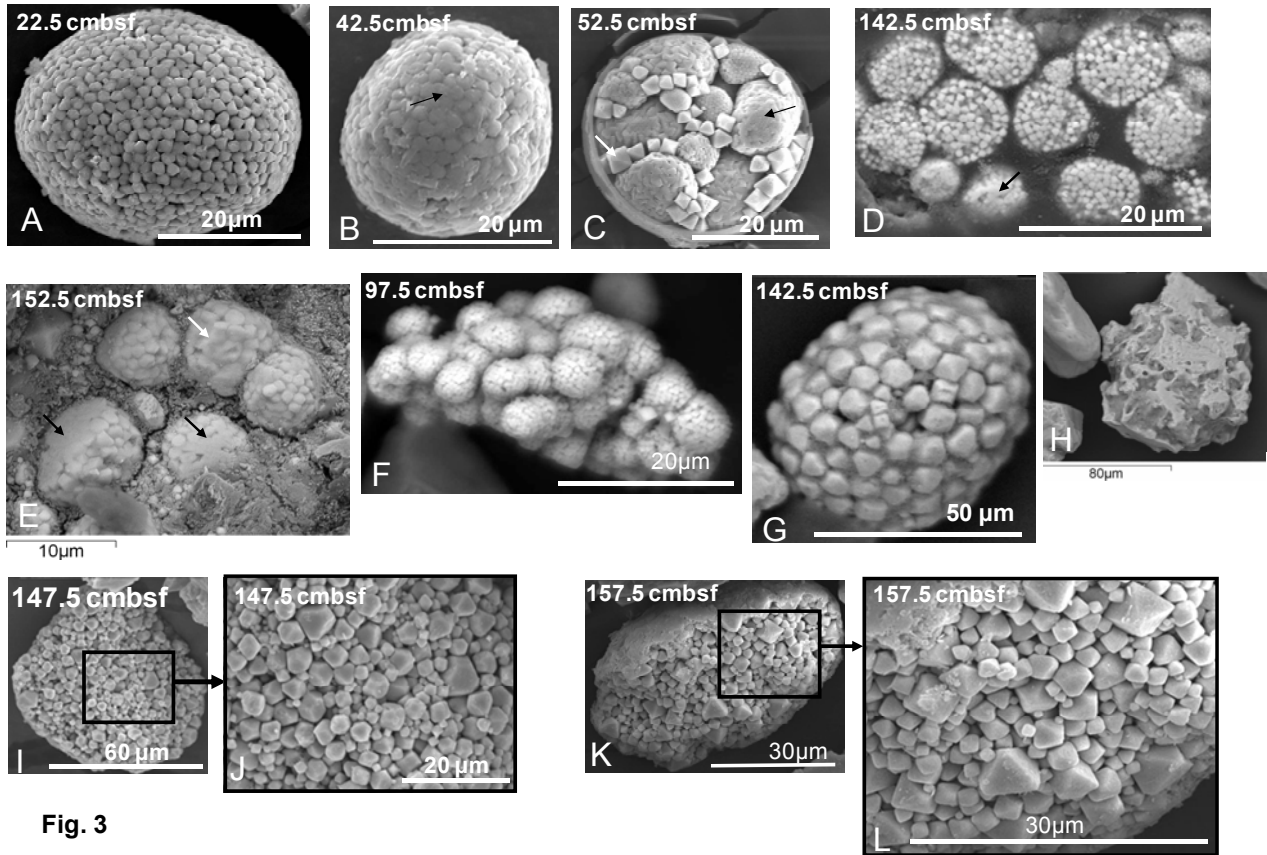


Fig. 3

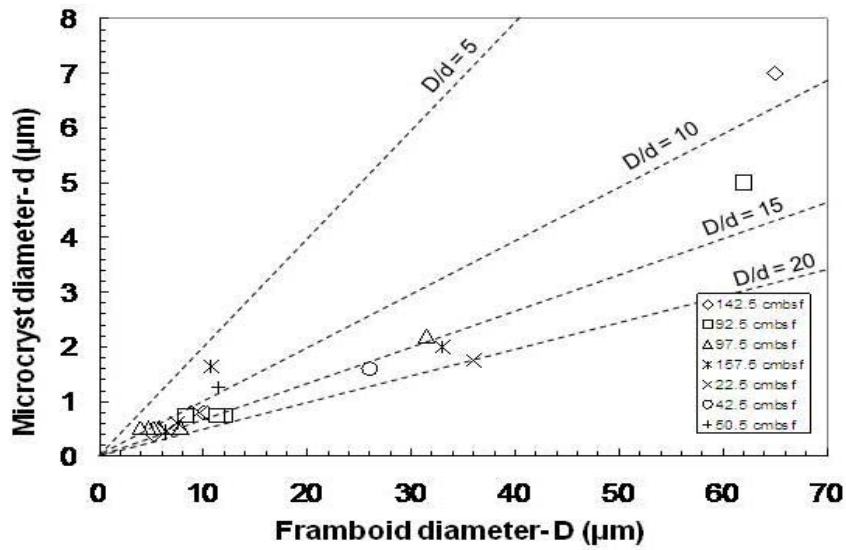


Fig. 4

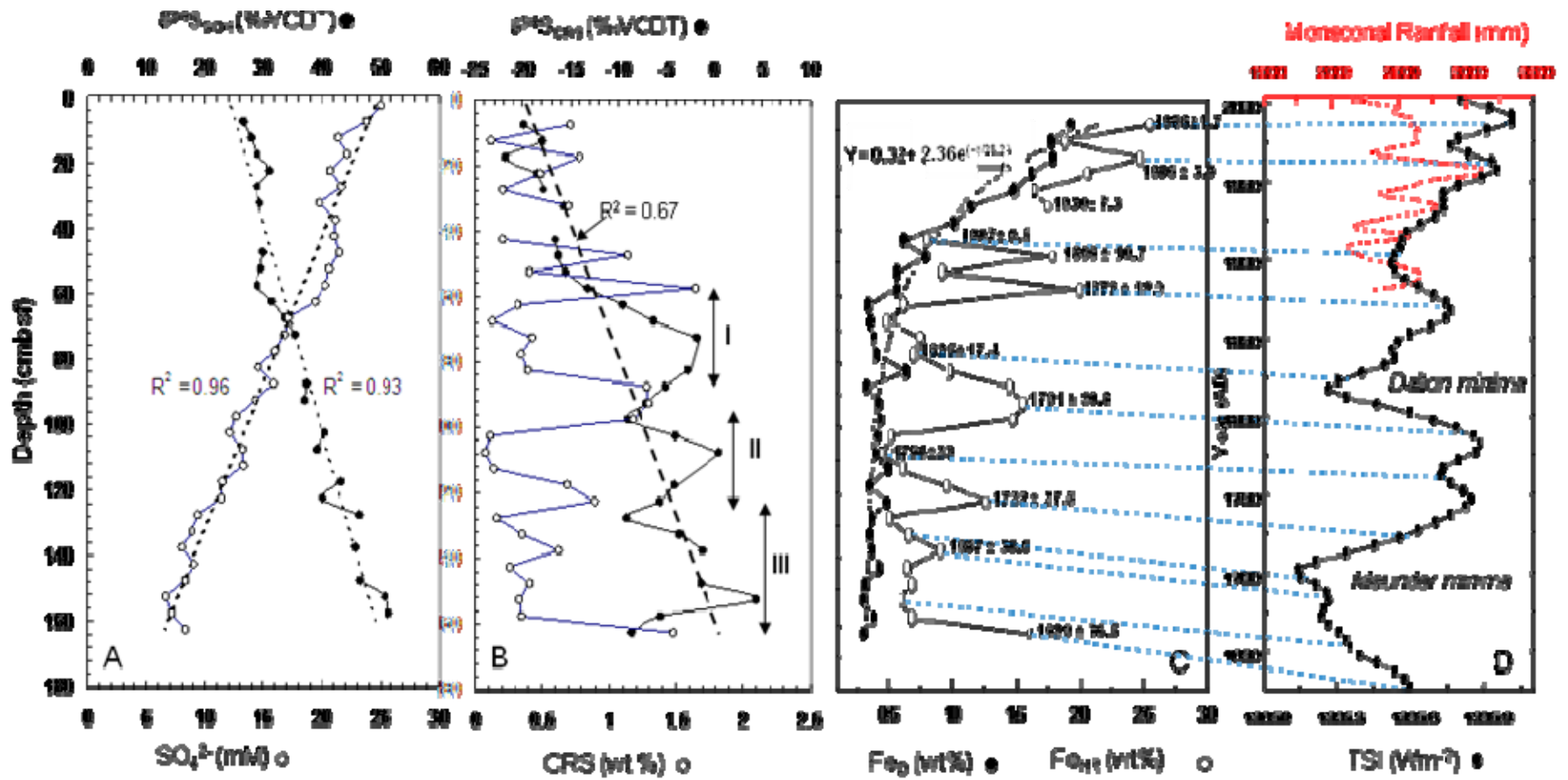


Fig.5

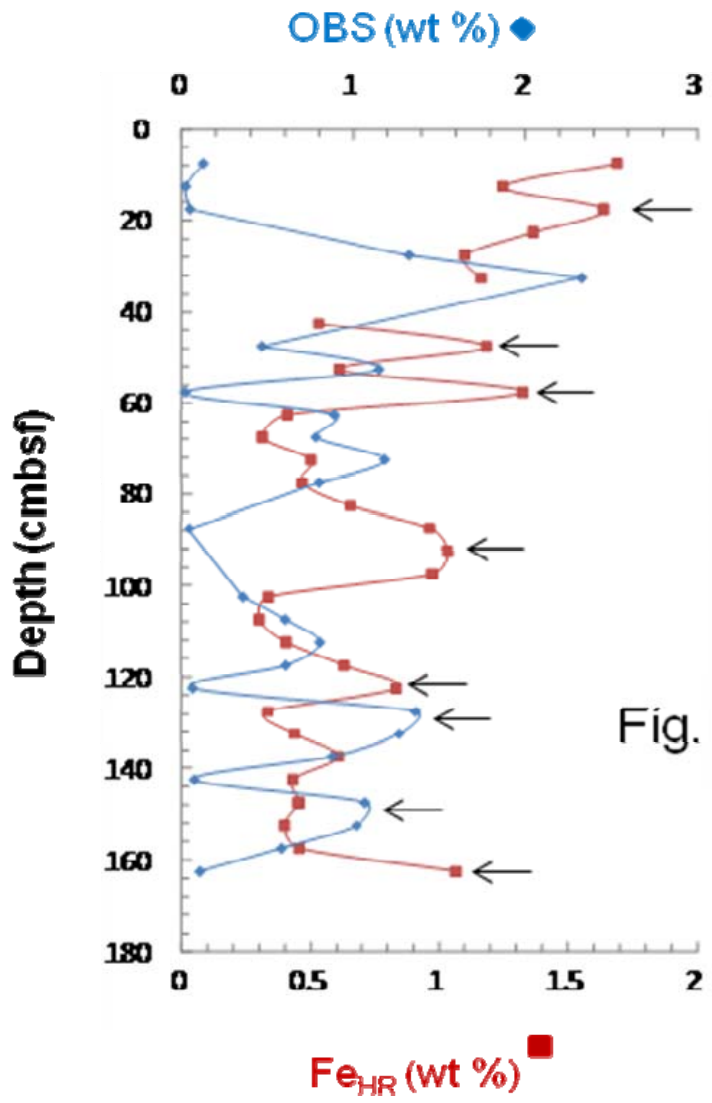


Fig. 6

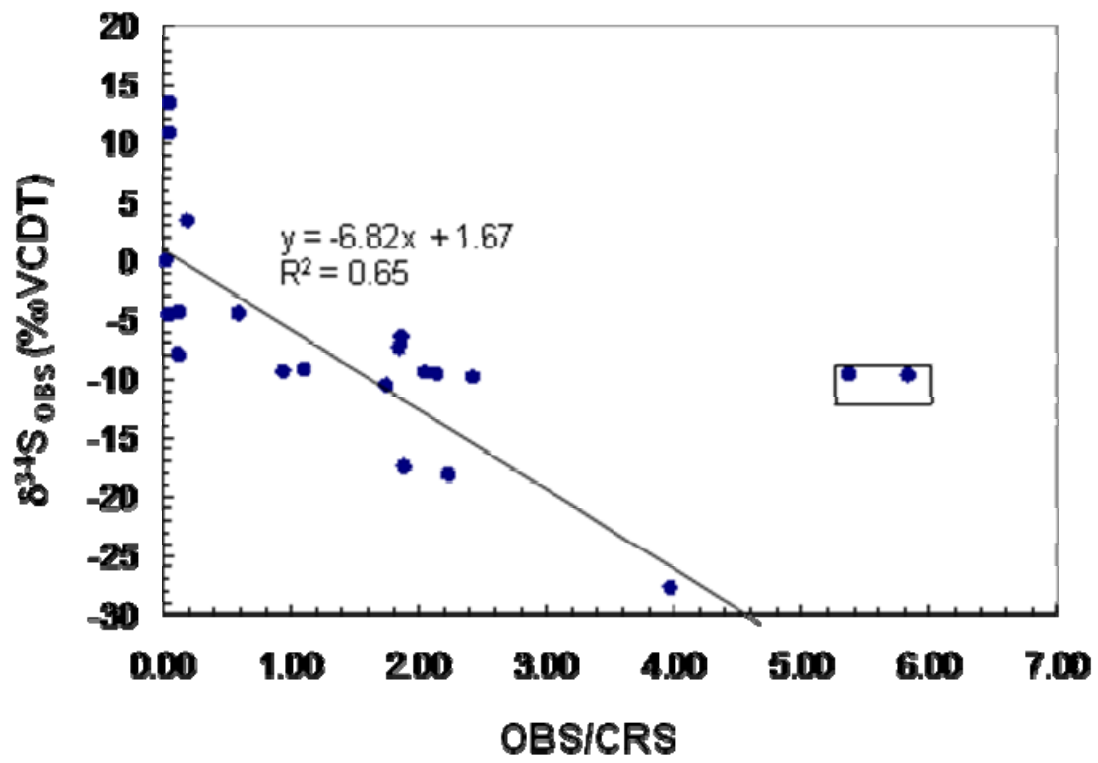


Fig.7

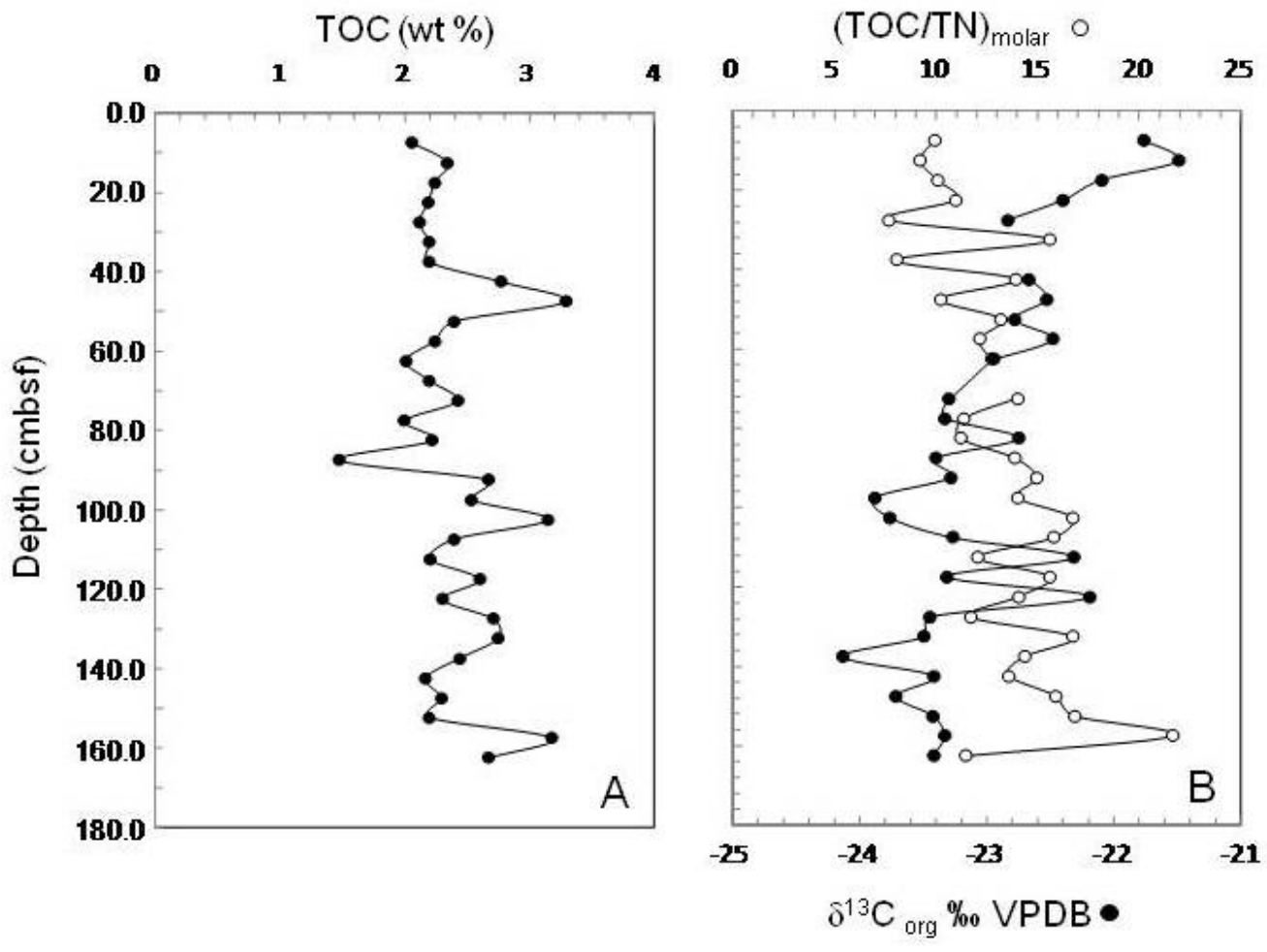
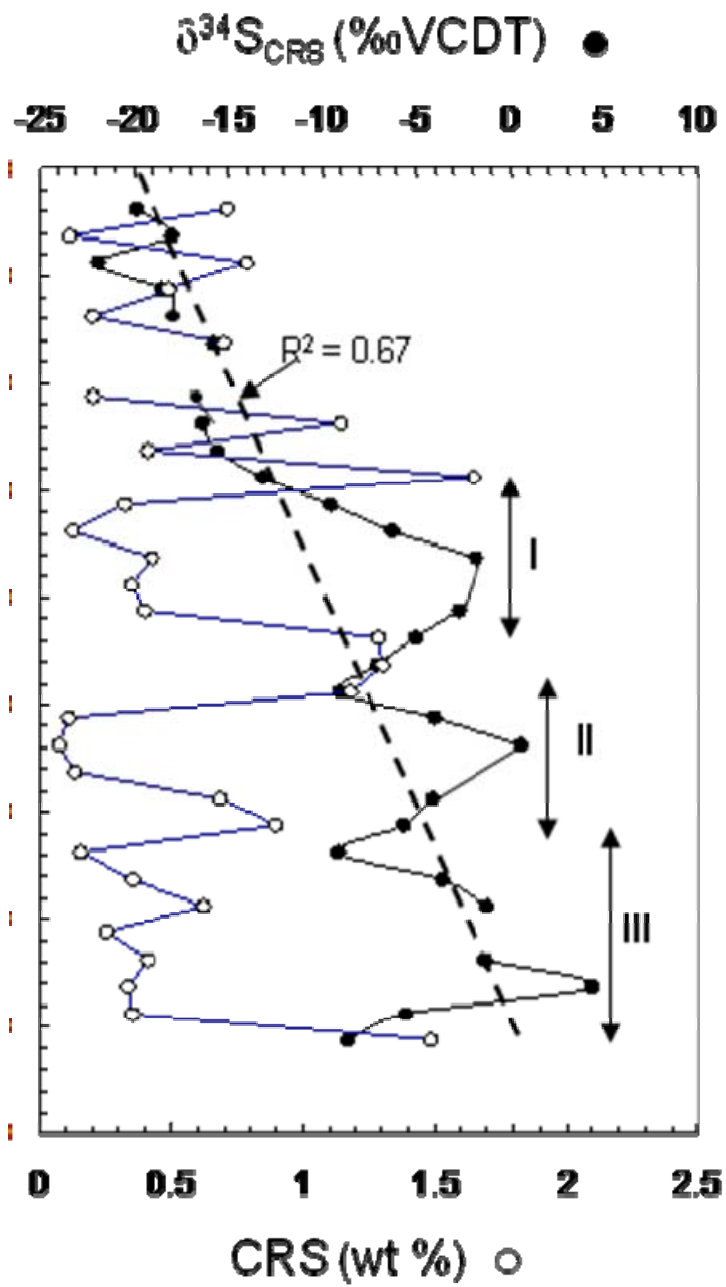
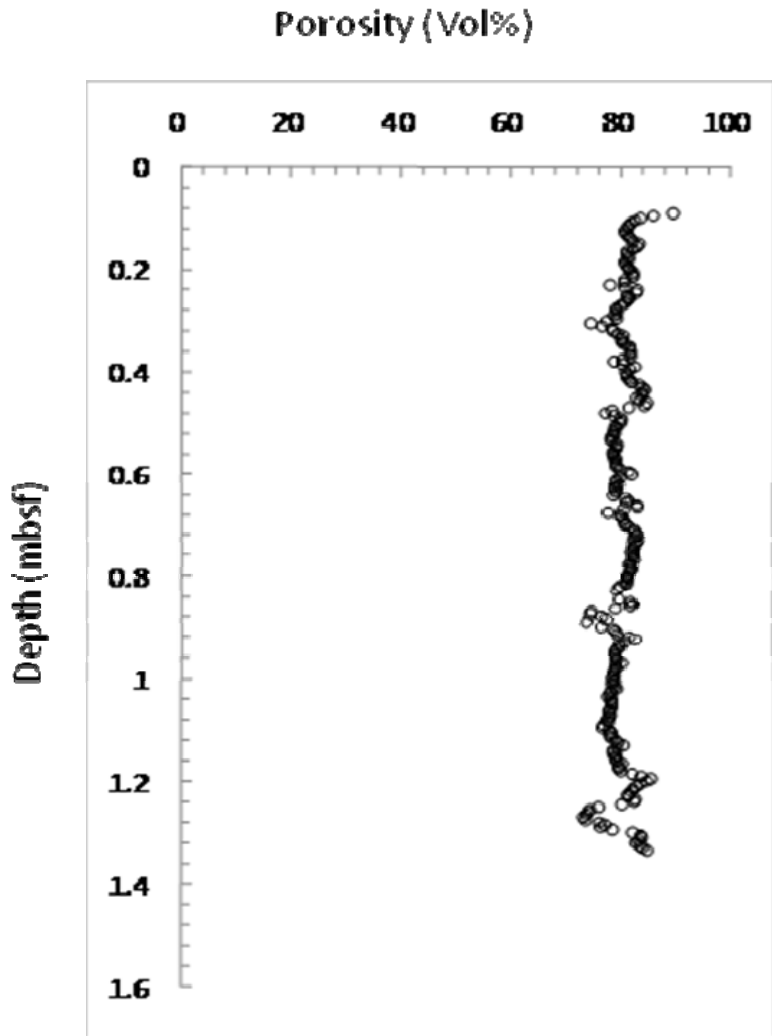


Fig.8

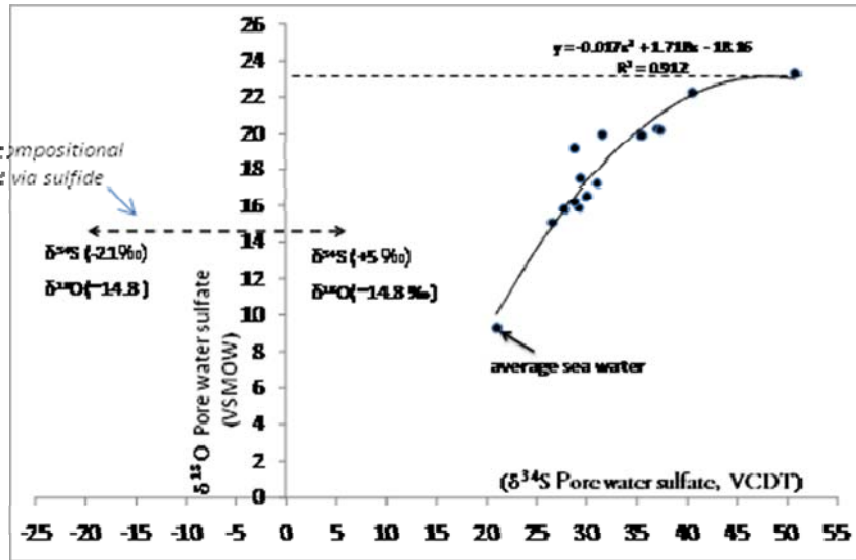


Graphical Abstract

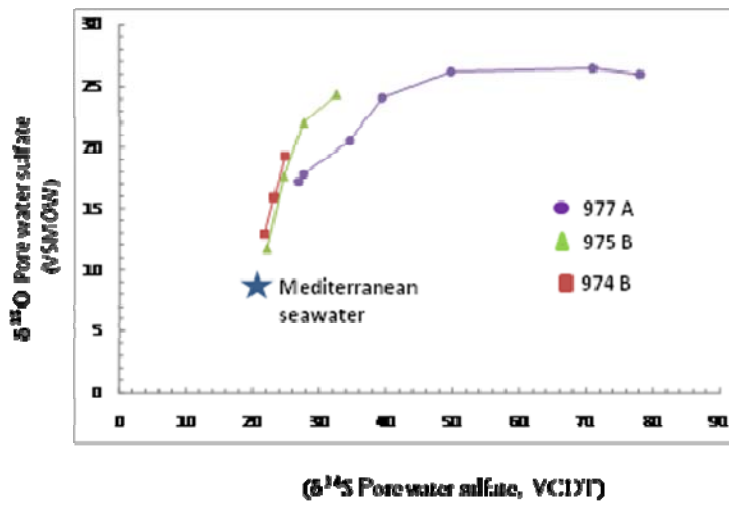


Supplementary Figure1

Possible $\delta^{34}\text{S}$ and $\delta^{33}\text{S}$ isotopic compositional range of sulfate produced via sulfide oxidation



A



Suppl. Fig2

B

$\delta^{33}\text{S}$ and $\delta^{34}\text{S}$ of residual sulfate in pore waters (modified after Bottcher et al., 1999)

Table-1

DEPTH (cm bsf)	Sulfate (mM)	AVS (wt %)	CRS (wt %)	OBS (wt %)	OBS/CRS	$\delta^{34}\text{S}_{\text{SO}_4}$ (PW) ‰VCDT	$\delta^{34}\text{S}_{\text{(CRS)}}$ ‰VCDT	$\delta^{34}\text{S}_{\text{(OBS)}}$ ‰VCDT	Fe _D (wt %)	Fe _{HR} (wt%)	Fe _T (wt%)	FeHR/FeT	TOC (wt%)	TOC/TN*	$\delta^{13}\text{C}_{\text{org}}$ ‰VPDB
2.5	25														
7.5	23.8		0.71	0.08	0.12	26.5	-19.9	-7.9	1.92	2.54	7.0	0.36	2.1	9.9	-21.8
12.5	21.4		0.12	0.01	0.13	27.8	-18	-4.3	1.77	1.88	6.8	0.28	2.3	9.2	-21.5
17.5	22.2		0.78	0.03	0.04	28.9	-21.9	-4.5	1.78	2.46	6.9	0.35	2.2	10.1	-22.1
22.5	20.8		0.49			31.1	-18.5	-16.6	1.62	2.05	6.6	0.31	2.2	11.0	-22.4
27.5	21.7		0.2019	0.89	4.38	28.9	-18.5		1.48	1.65	6.0	0.27	2.1	7.7	-22.8
32.5	19.8		0.70	1.55	2.23	29.3	-15.8	-18.05	1.14	1.75	6.7	0.26	2.2	15.6	
37.5	21.2								1.01		6.6	0.00	2.2	8.1	
42.5	21.1		0.20						0.62	0.80	6.7	0.12	2.8	13.9	-22.7
47.5	21.5		1.14	0.31	0.27	30	-16.4		0.79	1.78	6.4	0.28	3.3	10.2	-22.5
52.5	20.7	0.0012	0.41	0.77	1.89	29.5	-15.6	-17.4	0.56	0.92	6.1	0.15	2.4	13.2	-22.8
57.5	20.3		1.64	0.01	0.01	28.9	-13.2		0.56	1.99	7.2	0.27	2.2	12.1	-22.5
62.5	19.4	0.0025	0.32	0.59	1.85	31.5	-9.6	-7.3	0.34	0.62	6.4	0.10	2.0	12.7	-22.9
67.5	17.1		0.13	0.52	4.16	33.7	-6.3		0.36	0.47	6.4	0.07	2.2		
72.5	16.8		0.43	0.79	1.87	35.4	-1.9	-6.4	0.38	0.75	6.9	0.11	2.4	14.0	-23.3
77.5	16.0	0.0250	0.35	0.53	1.54				0.40	0.70	6.3	0.11	2.0	11.4	-23.3
82.5	14.5	0.0223	0.39					-2.8	0.64	0.98	6.2	0.16	2.2	11.2	-22.8
87.5	15.9	0.0043	1.28	0.03	0.02	37.3	-5.1	0.1	0.33	1.45	6.2	0.23	1.5	13.9	-23.4
92.5	14.3		1.30			37	-7.1		0.42	1.55	6.4	0.24	2.7	14.9	-23.3
97.5	12.7		1.18					-9.1	0.44	1.47	6.1	0.24	2.5	14.0	-23.9
102.5	12.1		0.11	0.24	2.14	40.5	-4.1	-9.5	0.41	0.51	6.3	0.08	3.2	16.7	-23.8
107.5	13.2	0.0019	0.07	0.40		39.1	0.5	-9.5	0.39	0.45	5.9	0.08	2.4	15.8	-23.3
112.5	13.3		0.14	0.54	3.96			-27.7	0.49	0.61	6.0	0.10	2.2	12.1	-22.3
117.5	11.5	0.0071	0.68	0.40	0.59	43.3	-4.2	-4.4	0.35	0.95	5.8	0.16	2.6	15.6	-23.3
122.5	11.4	0.0044	0.90	0.04	0.05	40.1	-5.7	10.9	0.47	1.26	6.1	0.21	2.3	14.0	-22.2
127.5	9.4		0.16	0.91		46.4	-9.2	-9.6	0.37	0.50	6.0	0.08	2.7	11.7	-23.4
132.5	8.9		0.35	0.85	2.42			-3.7	0.35	0.66	6.2	0.11	2.7	16.7	-23.5
137.5	8.0	0.0067	0.62	0.58	0.94	45.7	-1.3	-9.3	0.37	0.91	5.8	0.16	2.4	14.4	-24.1
142.5	9.1		0.25	0.05	0.19			3.5	0.43	0.65	6.0	0.11	2.2	13.6	-23.4
147.5	8.3	0.0063	0.41	0.71	1.74	46.5	-1.4	-10.5	0.32	0.68	5.8	0.12	2.3	15.9	-23.7
152.5	6.6	0.0010	0.33	0.68	2.04	50.8	4.3	-9.4	0.31	0.60	5.1	0.12	2.2	16.8	-23.4
157.5	7.1	0.0030	0.35	0.39	1.11	51.4	-5.6	-9.1	0.38	0.68	5.4	0.13	3.2	21.6	-23.3
162.5	8.3		1.48	0.07	0.05			-8.7	0.31	1.60	5.8	0.28	2.7	11.5	-23.4

TN (molar ratio)*

Supplementary Table-1

Depth (cmbfsf)	³⁴S (‰VCDT)	¹⁸O ‰ (VSMOW)
12.5	50.8	23.3
17.5	46.5	
27.5	45.7	
37.5	46.4	
42.5	40.1	
47.5	43.3	
57.5	39.1	
62.5	40.5	22.2
72.5	37	20.3
77.5	37.3	20.2
92.5	35.4	19.9
97.5	33.7	
102.5	31.5	20.0
107.5	28.9	
112.5	29.5	17.5
117.5	30	16.5
132.5	29.3	15.9
137.5	28.9	16.2
142.5	31.1	17.2
147.5	28.9	19.2
152.5	27.8	15.8
157.5	26.5	15.1